Materials Science and Engineering B 302 (2024) 117244

Contents lists available at ScienceDirect

Materials Science & Engineering B

journal homepage: www.elsevier.com/locate/mseb

Fluorine and nitrogen doping of zinc oxide to enhance dielectric storage of PVDF based particulate composites

Shuyang Chen [a,*], Vijay Kumar Thakur [b], Alexandros A. Skordos [a]

[a] School of Aerospace, Transport and Manufacturing, Cranfield University, Bedford MK43 0AL, UK
[b] Biorefining and Advanced Materials Research Centre, Scotland's Rural College (SRUC), Kings Buildings, West Mains Road, Edinburgh, UK

ARTICLE INFO

Keywords:
Polymer-ceramic particle composites
Dielectric spectroscopy
Relaxation
Dielectric storage
Thermal analysis

ABSTRACT

Polyvinylidene fluoride (PVDF) based polymer nanocomposites with ceramics as nanofiller have been investigated as a solution for energy storage devices due to their unique and attractive combination of processability and electrical properties. This work assesses two dopants (fluorine and nitrogen) for zinc oxide (ZnO) nanoparticles PVDF matrix composites as a means of improving dielectric properties targeting capacitive storage. Fluorine doping achieves improved performance compared to pure ZnO nanocomposites increasing the decomposition temperature by 15 °C to 463 °C with 15 wt% F-doped ZnO and reducing the weight loss by 4.2 %. The highest dielectric constant that can be achieved with the addition of fluorine is about 70 at room temperature, which is more than 3 times greater than that of pure ZnO nanocomposite. Nitrogen doping also enhances the permittivity of the nanocomposites at ambient temperature but limit enhancement at high temperature due to the lower activation energy.

1. Introduction

Dielectric materials have found many applications ranging from dielectric storage [1] to waveguides [2]. In dielectric capacitors, the fast charge/discharge of dielectric materials makes them a suitable energy storage device. Dielectric capacitors could be made by either ceramic or polymer. Various strategies to enhance dielectric performance has been proposed, for example, co-doping niobium and aluminum into TiO_2 [3] or introducing elemental deficiencies, such as that of bismuth in barium modified sodium bismuth titanate-barium strontium titanate (BNBT-BST) to enhance the dielectric constant of ceramics [4]. Co-polymers produced by grafting one dielectric polymer onto another have been used to enhance dielectric performance [5]. Current materials applied for energy storage are not limited to conventional dielectric polymers, for example, the application of 3D MXene has been used in supercapacitors [6]. Organic-inorganic hybrid materials have become one of the main options for dielectric energy storage devices [7] as introducing a filler in a polymer matrix can enhance the dielectric properties [8–10]. Polymer-ceramic hybrid materials are still a candidate with great potential to be used for electrodes of supercapacitors [11].

Fillers commonly used are ceramic particles with different structures, such as nanoparticles, nanorods, nanofibers or hollow structures [12–14]. Dielectric polymers, especially, PVDF and PVDF-based copolymers, play a very important role in storage applications due to their high breakdown strength, which results in greater energy storage density [15] and makes them a promising candidate as energy storage materials. Besides, polymers are generally easy to process and have low dielectric loss [16]. The energy density storage capacity of a linear dielectric polymer as an index to qualify the storage capacity of dielectric materials follows approximately a proportional relationship to its dielectric constant and to the square of its breakdown strength [17]. Consequently, the energy storage capacity of dielectric materials can be enhanced by either increasing the dielectric constant or the dielectric breakdown strength. In general, polymers have a relatively low dielectric constant and are easy to process, whereas ceramics have low breakdown strength, are difficult to process, and can attain high dielectric constant values [16]. Therefore, composites that combine the advantages of polymers and ceramics can play a crucial role in next generation energy storage devices [10,16,18–19].

Different ceramics have been used to produce polymer-based dielectric materials, such as $BaTiO_3$ (BTO) and calcium copper titanate (CCTO) [20–23]. The dielectric properties of composites of BTO with organic matrices present a dramatically increased dielectric constant by about 150 % compared to the neat matrix upon addition of 50 wt%

* Corresponding author.
E-mail address: shuyang.chen@cranfield.ac.uk (S. Chen).

https://doi.org/10.1016/j.mseb.2024.117244
Received 5 October 2023; Received in revised form 23 January 2024; Accepted 5 February 2024
Available online 20 February 2024

ceramic particles [21] and can be further improved by surface modification of the particles[20]. The effect of ZrO_2 on the dielectric constant of polyvinylidene fluoride-co-chlorotrifluoroethylene (PVDF-CTFE) based nanocomposites is moderate due to the relatively close dielectric constants of matrix and particles; an improvement in the dielectric constant of about 20 % is observed when 17 wt% of nanoparticles is added [22]. The addition of CCTO results in significant improvements in dielectric constant exceeding a 10 fold increase when 40 vol% is added to a polymer matrix [23]. ZnO nanoparticles have also been used, motivated by the strong interface they form with host polymers [24,25]. The interface between organic and inorganic materials is key in enhancing the dielectric properties and overall quality of the material; incompatibility between ceramic nanoparticles and the polymer matrix can lead to aggregation, porosity and voids in the nanocomposites which influence the dielectric properties and other material quality metrics adversely [16].

As a semiconductor, ZnO has very attractive properties such as exceptional optical, electronic and electrochemical response and it is environmentally friendly [26]. As a result of its piezoelectric properties, ZnO has been considered as a candidate to modify high frequency surface acoustic wave devices used as sensors to detect certain gases such as fluorine or methanol [27] with its selectivity enhanced by coating zeolitic imidazolate onto ZnO nanorods [28]. Modified ZnO can also be used as energy storage material to fabricate self-charging supercapacitors [29].

The high exciton binding energy (60 meV) and wide bandgap (3.37 eV) of ZnO allow it to operate at high voltage, frequency and temperature [30]. Improved dielectric constant values of composites containing ZnO nanoparticles have been reported; the permittivity of nanocomposites with 30 wt% ZnO is about 30 % greater than that of pure PVDF [31]. Surface modification of ceramics has been investigated to improve further the dielectric properties of nanocomposite dielectric materials. A greatly enhanced dielectric constant (about 100 % increase) can be achieved with only 10.8 vol% addition of particles after dispersing $BaTiO_3$ nanofibers in a dopamine hydrochloride aqueous solution [19]. Doping the particles with metal ions can also be an effective option; nanocomposites containing Ni-doped BaTiO3 present ultra-high dielectric properties [32]. ZnO has also been used as a separator of arrays of electrodes to fabricate low cost and environmentally friendly supercapacitors [29].

In addition to metal ions, fluorine and nitrogen are considered as an attractive candidate to maximise the energy storage ability of dielectric materials. Fluorine and nitrogen doping have been investigated with the aim of improving the electrical and optical properties of ceramics. Fluorine has been applied to energy storage materials previously. For example, fluorine-doped graphene-based supercapacitors achieve a significantly higher energy and power density than pristine graphene [33]. Fluorine has also been employed to enhance electrical conductivity [34], by increasing the charge carrier concentration, which could also influence dielectric properties. Surface fluorinated waste rubber powder has been used to fabricate triboelectric nanogenerators [35]. Fluorine has also been used to dope non-metal polymeric semiconductors such as graphitic carbon nitride to enhance the optical, electric and emission properties [36]. More importantly, fluorine doped SnO_2 has shown an improved dielectric constant [37]. Nitrogen is also an attractive candidate for doping. Similarly, to fluorine, it has been shown that N-doped ZnO achieves a higher dielectric constant [38].

There is limited research on the thermal and dielectric properties of fluorine/nitrogen-doped nanocomposites and on using non-metallic dopants in general to enhance the dielectric constant reported so far in the literature. This study focuses on the investigation of thermal and dielectric properties of polymer-based nanocomposites with fluorine/nitrogen doped ZnO nanoparticles to assess the feasibility of doping with these elements to improve the performance of storage devices based on PVDF-ceramic composites. This can facilitate understanding of how dopants influence the behavior of the nanocomposites. This is the first-time formulation and synthesis of polymer ceramic nanocomposites using fluorine/nitrogen doping of the nanoparticles is reported. In addition, the application of fluorine can improve the compatibility between the ZnO and PVDF as PVDF has also functional groups with fluorine and the doping of the particles can improve the interface coupling. The approach followed here differs significantly from strategies utilised previously in the literature to improve the compatibility between the matrix and nanofiller, such as the use of surfactants [39] which can have adverse effects with respect to leakage currents. Previous work focusing on improving thermal properties of polymer based nanocomposites is based on use of multiple nanofillers and surfactant [40] , resulting in complex synthesis. The use of doping in this work, offers an alternative route for improving thermal stability that can be implemented using a simple synthesis procedure.

2. Materials and experimental methods

2.1. Chemicals

Zinc nitrate hexahydrate ($Zn(NO_3)_2{\cdot}6H_2O$ CAS: 10196–18-6, MW ~ 297.49) and potassium hydroxide (KOH CAS: 1310–58-3, MW ~ 53.11) powders were supplied by Sigma Aldrich [41–42] and used directly without any further milling before adding into distilled water. Ammonium fluoride (Sigma Aldrich, NH_4F, CAS: 12125–01-8, MW ~ 37.04 [43]) with ACS reagent was used as source of fluorine in the form of powder. Synthesis level urea (Sigma Aldrich, CN_2H_4O, CAS: 57–13-6, MW ~ 60.06 [44]) was used as the source of nitrogen and was also used as powder directly. Polyvinylidene fluoride (PVDF, CAS: 24937–79-9, MW ~ 534000 by GPC [45]) in powder form with chemical formula $(CH_2CF_2)_n$ used as the main material for the film and BioReagent Dimethyl Sulfoxide (DMSO $(CH3)_2SO$, CAS: 67–68-5, MW ~ 78.13 [46]) liquid used as the solvent applied for film preparation was also supplied by Sigma Aldrich. Conductive silver liquid paint (RS Components 186–3600 [47]) was used for coating samples for dielectric measurements.

2.2. Synthesis

2.2.1. Synthesis of ZnO and fluorine/nitrogen-doped ZnO

The synthesis procedures of the nanoparticles follow a previous study [48], zinc nitrate (0.1 mol) aqueous solution (500 ml) and potassium hydroxide (0.2 mol) aqueous solution (500 ml) were stirred at room temperature for 2 h separately. The agent solution was then added into the precursor solution drop wisely while the precursor solution was kept stirring during the process. The whole process lasted about 25 min. The final solution was stirred for about 1 h, then sealed and settled for 24 h. After removing the suspension solution, the precipitate was obtained by using centrifugation (Heraeus Megafuge 8) for 10 min at 4500 rpm; the collected precipitate was washed in distilled water and centrifuged again to wash away impurities. This process was repeated three times and ethanol was used in the last step to ensure impurities are removed and the pH value of the particles was maintained at about 7. The precipitate was then dried in a vacuum oven (THCHEM Model DZF-6050) at 90 °C for 12 h in standard atmosphere to convert the $Zn(OH)_2$ to ZnO. The dried powder was heat treated at 500 °C for 3 h in a furnace (Severn Science-TG38.2.1Z.F) to eliminate any organic residue and ensure purity of the nanofiller.

The synthesis process of fluorine-doped and nitrogen-doped ZnO is identical to the process used for the synthesis of pure ZnO particles with the only difference being the addition of ammonium fluoride powder and urea powder into the precursor solution before mixing for F- or N-doping respectively. The molar ratio of dopant to Zn was 10 %. Therefore, 0.01 mol of ammonium fluoride or 0.005 mol of urea powder was weighted and mixed with zinc nitrate powder before dissolving into distilled water. The mixed solution was sealed and settled overnight for precipitation followed by stirring in distilled water for 30 min and

centrifugation to obtain the washed precipitates. After drying in the oven, the powder was annealed in the furnace.

2.2.2. Preparation of nanocomposite films

Polymer and nanocomposite films were prepared by using a 11 cm × 11 cm glass plate as the substrate with silicone rubber forming a frame containing the solution. To make sure the final product could achieve the required thickness, the solution was only deposited onto the centre area of the substrate which had dimensions of 10 cm × 10 cm, with the rest of the area was covered by the rubber frame. The rubber frame, a top steel plate and the glass substrate were clamped to make sure the solution does not leak during the heating process.

The nanocomposite material was formulated by dissolving 2 g of PVDF powder into 40 ml of DMSO and the corresponding amount of ceramic powder into 5 ml of DMSO. The PVDF solution and the ceramic mixture were stirred for 2 h at 70 °C separately and then mixed gradually. After mixing, the solution was stirred for 2 h at 70 °C and then sonicated (Clifton SW3H) for 30 mins to achieve better mixing. The film solution was sealed in a 100 ml beaker before immersion into water for sonication. The solution was deposited onto the clamped glass preparation substrate, then heated at 90 °C for 24 h to evaporate the solvent completely. The film could be easily peeled off from the substrate after heating.

The molar ratio between the dopant and Zn was fixed at 10 %, and the weight fraction of the pure and doped ZnO powder was 5 wt%, 10 wt % and 15 wt%. The films were coated with conductive silver paint on both sides, with the coating area kept the same as the size of the electrodes used in dielectric measurements.

2.3. Characterisation

Thermal degradation and stability analysis was carried out using a Thermogravimetric Analyser (TGA-TA instrument Q500) under nitrogen atmosphere. The maximum temperature reached 800 °C and the heating rate was 10 °C/min. A Differential Scanning Calorimeter (DSC-TA instrument Q200) was used to investigate the thermal transitions of the nanocomposites. The tests were performed in nitrogen atmosphere. DSC samples were heated from 60 °C to 250 °C with a heating rate of 10 °C/min and then kept at 250 °C for 2 min. After the isothermal segment, the samples were cooled down to −60 °C with a cooling rate of 10 °C/min and then heated again to 250 °C with the same heating rate. The purpose of the first heating and isothermal segment is to eliminate the thermal history of the materials. The melting and crystallisation temperature were obtained from the cooling and the second heating process. The test samples for TGA and DSC were cut from the uncoated part of the film without any further processing.

X-ray diffraction (XRD Siemens D5005) was used to investigate the crystal structure of the nanocomposites and the influence of the dopants. The experiments were operated with a sample size of about 0.5 cm^2 and wavenumber of 1.54 cm^{-1}. Scanning Electron Microscopy (SEM) was carried out using a SEM Tescan S8000 microscope. All the films and powders were gold-coated prior to SEM analysis using a Quorum Turbo sputter coater targeting a coating thickness of 10 nm.

Dielectric tests were carried out using a Solatron SI1260 Frequency Analyzer (FRA). The tests were operated in the frequency range of 10^1-10^6 Hz scanned in a logarithmic scale using 29 points. In all experiments the excitation voltage was 1 V. Measurements were carried out at about 25 °C, 50 °C, 75 °C and 100 °C. Each isothermal measurement had a duration of 15 min to stabilise the temperature. A k-type thermocouple was attached to the measuring cell to monitor and record the temperature. An in-house code built in LabView was utilised to acquire synchronised dielectric and temperature data. The nanocomposite films with a size of 10 cm × 10 cm were placed between two circular copper electrodes connected with the FRA. The diameter of the upper and bottom electrodes were 5 cm and 8 cm respectively with a thickness of 8 mm. The electrodes and sample assembly was placed on a Sindanyo high temperature insulation board with thickness of 2 cm during the measurement. The upper electrode covered the coating area of the nanofilms and the two electrodes were completely separated by the nanofilm.

The FRA provides raw results in the form of capacitance and resistance in an assumed parallel circuit. The dielectric constant can be calculated using:

$$\varepsilon' = \frac{C}{\varepsilon_0}\frac{d}{S} \tag{1}$$

where C is the measured capacitance, ε_0 is the constant of free space which is 8.854 × 10^{-12}F/m and d and S are the thickness of the film and coated area respectively. The dielectric loss can be calculated as:

$$\varepsilon'' = \frac{1}{\varepsilon_0 R\omega}\frac{d}{S} \tag{2}$$

where R is the measured resistance, and ω is the angular frequency. To facilitate visualisation of relaxations, the imaginary electric modulus was also calculated as follows:

$$M'' = \frac{\varepsilon''}{\varepsilon'^2 + \varepsilon''^2} \tag{3}$$

The dataset underlying this study is available at the Cranfield online research data repository [49].

3. Results and discussion

3.1. Thermal decomposition

The thermal degradation behavior of nanocomposites with a heating rate of 10 °C/min and 5 wt% of doped and pure nanofiller is presented in Fig. 1. Pure PVDF presents a two-step decomposition. The first decomposition, which has an onset at around 439 °C, is mainly attributed to chain-scission and causes a 76.6 % weight loss, due to the breaking of carbon-hydrogen or fluorine leading to the disassembly of the polymer structure [50–51]. The second step of degradation has an onset temperature of 487 °C and is attributed to the polyenic sequence generated in the first degradation step undergoing scission after the formation of aromatic molecules [50,52]. The TGA curve shifts to a higher decomposition temperature with the addition of 5 wt% ZnO, whilst the shift is greater with the addition of dopants in the nanoparticles.

Table 1 presents the onset and inflexion temperature (T_{onset} and T_{max}) of all the nanocomposites investigated. The decomposition temperature of PVDF + ZnO is higher than that of the neat PVDF and gradually increases with the ZnO content; the inflection point (T_{max}) also increases to 467 °C with 5 wt% nanofiller and to 471 °C and 474 °C for the materials with 10 wt% and 15 wt% ZnO respectively. The shift of the curves shows that the nanofiller improves thermal stability compared to the neat PVDF polymer. The degradation temperature does not increase significantly when the ZnO amount changes from 10 wt% to 15 wt%, showing that the improvement in thermal stability of the nanocomposites becomes saturated with increasing content. Both fluorine and nitrogen doped nanocomposites present decomposition curves shifted to greater temperatures, indicating that the addition of dopants improves the thermal stability of the materials. The decomposition onset temperature increases to 458 °C, 461 °C and 463 °C with the increase of fluorine doped nanofiller. N-doped nanocomposites present the highest decomposition onset temperature among all the nanocomposites, which reaches 465 °C. The nanocomposites containing F-doped ZnO exhibit increased inflection temperature, particularly when 5 and 10 wt% of particles are added, which is around 471 °C and 475 °C respectively. Further addition of nanoparticles does not increase the inflection temperature further, as the inflection temperature of both doped and undoped nanocomposites is 475 °C when 15 wt% nanofiller is added. When 5 wt% of N-doped ZnO is added, the inflection temperature of the

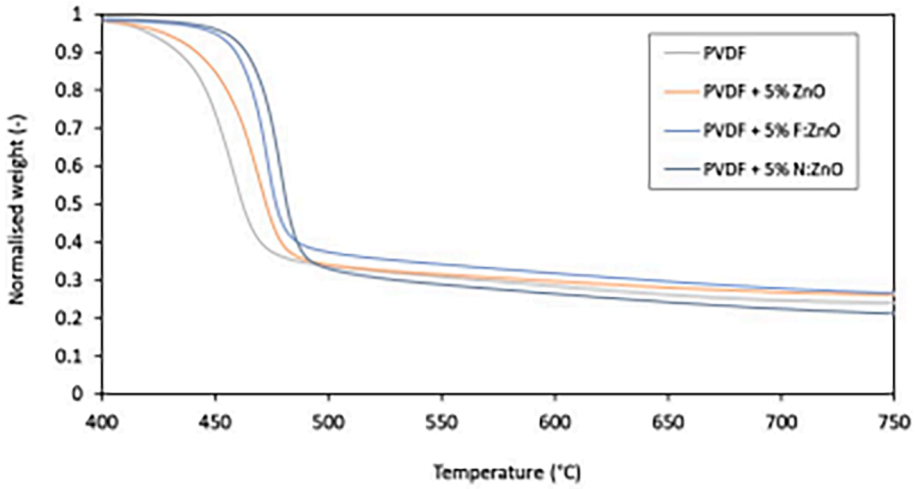

Fig. 1. TGA curves of PVDF and nanocomposites with and without doping.

Table 1
Degradation parameters of PVDF and nanocomposites with and without dopants.

Material	Total loss	T_{onset}°C	T_{max}°C	PVDF loss
Pristine PVDF	0.766	439	459	0.766
PVDF + 5 % ZnO	0.744	443	467	0.783
PVDF + 10 %ZnO	0.715	448	471	0.795
PVDF + 15 % ZnO	0.674	448	474	0.794
PVDF + 5 % F: ZnO	0.739	458	471	0.778
PVDF + 10 % F:ZnO	0.657	461	474	0.731
PVDF + 15 % F:ZnO	0.632	463	475	0.744
PVDF + 5 % N: ZnO	0.794	465	479	0.836
PVDF + 10 % N: ZnO	0.690	464	476	0.766
PVDF + 15 % N: ZnO	0.681	465	475	0.802

nanocomposite increases to 479 °C, which is higher than the inflection temperature of the pure ZnO nanocomposite with the same loading. This represents the highest inflection temperature among all nanocomposites. Further addition of N-doped nanoparticles reduces slightly the temperature to 476 °C and 475 °C with 10 wt% and 15 wt% of nanofiller, whereas the inflection temperature of pure ZnO material with 15 wt% doping is also 475 °C. The inflection temperature of all nanocomposites with and without dopant is around 475 °C when 15 wt% of nanofiller is applied. This implies that 475 °C is the plateau temperature of the nanocomposites; further addition of dopant does not increase the maximum degradation temperature further.

Table 1 presents the final weight loss and matrix weight loss for all materials. Since the degradation of PVDF occurs by bond scission and rupture of C-H and C-F bonds by thermal decomposition, it generates double C-C bonds. The weight loss in the first degradation stage is accompanied by removal of HF. The mass loss becomes slower in the second stage, and the degradation generates tar; therefore, the whole degradation process of PVDF generates HF, tar and char [53]. The removal of HF is followed by carbonisation of the polymer and then cyclisation of the released species. The greater temperature leads to a fully carbonised residue by polymer crosslinking [54], which explains why the second stage occurs at high temperatures. The total weight loss decreases from 76.6 % for PVDF to 74.4 % with 5 wt% of ZnO and is reduced further to 71.5 % and 67.4 % when 10 wt% and 15 wt% of ZnO is added. However, the polymer weight loss shows the opposite trend. The polymer weight loss with ZnO is around 79.5 % which is 2.9 % higher than that observed in pure PVDF. Fluorine doped nanocomposites present lower weight loss than pure ZnO nanocomposites and both total weight loss and polymer weight loss decrease further with the increase of fluorine doped nanofiller. This could be attributed to the introduction of extra fluorine that may help the formation of C-F bonds and delay the elimination of HF. Also, the presence of fluorine in the particles can help the ZnO nanoparticles to build a stronger interface with the polymer and restrict chain movement, which results in a reduction of PVDF weight loss. Furthermore, fluorine may also form H-F bonds which have greater bonding dissociation energy (136.2 Kcal/mol) than F-Zn (88 kcal/mol) and O-Zn (67.9 kcal/mol) [55]. The weight loss of N-doped nanocomposites with increasing amount of nanoparticles is consistent with the results obtained for pure ZnO nanocomposites. The total weight decreases with the nanofiller, but polymer weight loss increases. N-doped nanocomposites also present the highest total weight loss and polymer weight loss among all nanocomposites studied, around 79.4 % and 83.6 % respectively. This indicates that the addition of nitrogen may affect negatively the interface between Zn and O by occupying interstitial positions into the ZnO structure leading to oxygen loss.

3.2. Thermal transitions

Fig. 2 illustrates the melting and crystallisation behavior of pristine PVDF and nanocomposites with and without dopant measured by Differential Scanning Calorimetry (DSC). The DSC curves of the nanocomposites show a single melting peak, which is narrower than the peak of pure PVDF. This is due to the fact that ZnO acts as a heterogeneous nucleating agent and facilitates the formation of more uniform but smaller lamellae which can melt entirely in a heating cycle [56]. The melting/crystallisation temperature and enthalpy of the different materials are summarised in Table 2. The melting temperature increases with the addition of ZnO and then decreases slightly with further addition of greater amount of ZnO nanoparticles. The melting enthalpy increases monotonously with increasing ZnO content. Also, both the crystallisation temperature and enthalpy increase with the increase of nanoparticle content. The crystallinity of the nanocomposites is higher than that of the pure PVDF and is enhanced further by the increase of nanofiller amount.

The shift of the melting temperature to greater values with the addition of ZnO is a consequence of the nanoparticles promoting crystallisation of PVDF by acting as a nucleating agent. Meanwhile, the observed reduction in melting temperature with increasing ZnO content is attributed to the facilitation of crystallisation of PVDF by ZnO, which results in smaller crystallites that can be melted at lower temperature [57]. The increase of melting enthalpy indicates that although the crystallite size decreases with ZnO loading, the crystallites amount grows. The increase of crystallisation temperature and enthalpy represent the enhanced interface energy when the nanofiller is added. The crystallinity increases with the nanoparticles amount which evidences

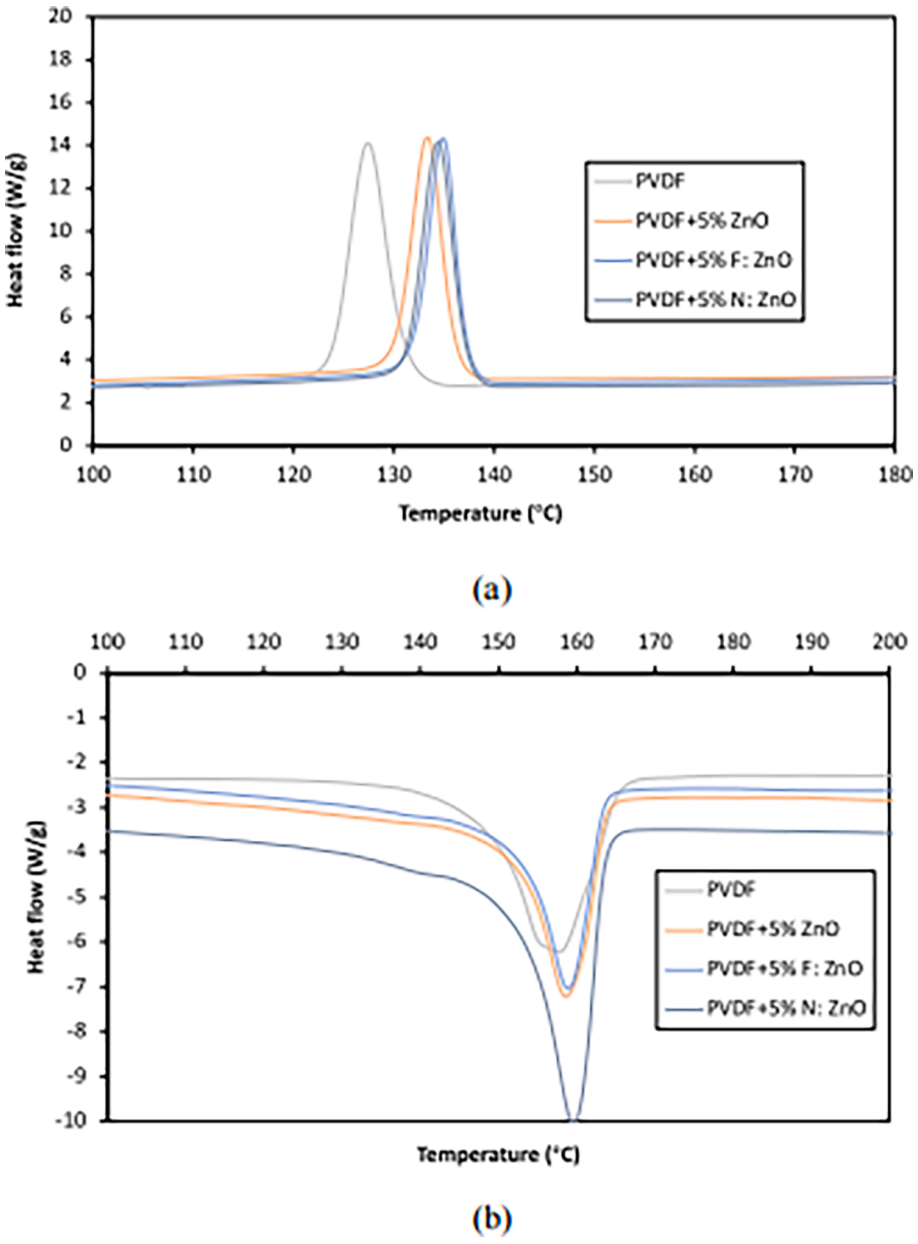

Fig. 2. Calorimetric response during melting (a) and crystallisation (b) of PVDF and nanocomposites with and without dopants.

Table 2
Melting/crystallisation temperature and enthalpy of PVDF and nanocomposites with and without adding dopants. Crystallinity computed using a PVDF crystallisation enthalpy of 104.7 Jg^{-1} [58].

Material	Tm°C	ΔHmJ/g	Tc°C	ΔHcJ/g	ΔXc
Pristine PVDF	157.8	43.6	127.7	45.7	45 %
PVDF + 5 % ZnO	158.7	50.6	133.4	47.2	47 %
PVDF + 10 %ZnO	158.5	54.2	134.1	52.2	55 %
PVDF + 15 % ZnO	157.9	58.9	133.2	55.5	56 %
PVDF + 5 % F: ZnO	158.8	55.5	134.8	53.9	54 %
PVDF + 10 % F: ZnO	158.8	65.1	135.1	58.0	61 %
PVDF + 15 % F: ZnO	158.8	76.0	135.9	65.1	65 %
PVDF + 5 % N: ZnO	159.7	57.7	134.4	48.5	49 %
PVDF + 10 % N: ZnO	158.2	44.2	130.6	42.4	45 %
PVDF + 15 % N: ZnO	158.5	39.8	132.9	42.5	48 %

their influence in promoting crystallisation of PVDF by acting as a nucleation agent [56].

Nitrogen and fluorine doping influence thermal transitions in nanocomposites in different ways. As reported in Table 2, the addition of F-doped ZnO results in an increase of melting temperature and enthalpy compared to pure ZnO nanocomposites. The melting temperature remains constant with various nanofiller concentrations, whilst the melting enthalpy increases as the concentration of F-doped ZnO increases. The crystallisation temperature of F-doped films follows the same trend as the melting temperature and enthalpy and represents the highest values among the materials with the same amount of nanoparticles. The constant melting temperature implies that the crystal size of F-doped nanocomposites does not change as a function of nanoparticle content. The increase of melting enthalpy indicates that the addition of F-doped nanoparticles further enhances the crystallite number. The greater crystallisation enthalpy reflects higher crystallinity which can be attributed to greater interfacial energy of the F-doped nanoparticles. The N-doped nanocomposite with 5 wt% nanoparticles presents the highest melting temperature among all the materials; further addition of nanofiller decreases the melting temperature as well as the melting enthalpy. Similarly to melting, the crystallisation

temperature as well as the crystallisation enthalpy of the N-doped nanocomposites decrease with nanoparticle content. The higher melting temperature of N-doped nanocomposite indicates that the N-doped nanocomposites with 5 wt% nanofiller has the largest crystal size. However, further addition of N-doped ZnO does not enhance further the crystallisation of nanocomposites. The reduction of crystallisation temperature and enthalpy indicates that nitrogen doping affects the interfacial energy and nucleation of the nanocomposites negatively.

3.3. Crystal structure and morphology

Fig. 3 illustrates the XRD spectra of neat PVDF and of its nanocomposites which reflect the semi-crystalline structure of the polymer and crystalline structure of the nanofiller. The XRD peaks can be used to deduce the change of the lattice parameters and to identify how the dopants affect the crystal structure of the nanocomposite. This is also linked to potential effects on dielectric properties as a result of changes in the crystal structure.

Pure PVDF has three main peaks located at 20.29°, 18.48° and 39.37° which correspond to the (1 1 0), (0 2 0) and (1 3 2) planes, and a relatively weak peak at 41.65° corresponding to the (−2 2 1) plane. The strength of the (1 1 0) and (0 2 0) plane peaks indicate that pristine PVDF is dominated by α phase [59]. The (2 0 0) plane, which is characteristic of the β phase of PVDF, located at 36.39° and the (1 1 1) plane located at 22.58°, which is present in the α phase [60], can also be observed. The PVDF peaks do not undergo any distinct shift. In addition to the main peaks the relative weak peak corresponding the plane (−2 2 1) can still be observed in the spectrum. After addition of 5 wt% of ZnO nanoparticles, the spectrum shows three additional peaks at 31.76°, 34.50° and 36.23° respectively, indicating the hexagonal structure of ZnO [61] as well as peaks at 47.54°, 56.57°, 62.85°,67.92° and 69.05°, and a weak peak located at 66.32°. The sharpness of the peaks indicates that a fine crystalline structure of ZnO has been achieved. The addition of dopants does not generate any additional peaks, showing that the dopants do not prominently affect the crystal structure of the nanocomposites. With fluorine doping, the three main PVDF peaks which correspond to the (1 1 0), (0 2 0) and (1 3 2) planes shift to 20.45°, 18.72° and 39.22° respectively, whilst the main ZnO peak shifts to 31.99°. The other two main peaks at 34.50° and 36.23° do not show any shift. The rest of the peaks corresponding to ZnO present an overall right shift. The peaks shift to 47.69°, 56.66°, 62.91°, 68.00° and 69.22° with the addition of fluorine, while the relative weak peak also shifts to the right to 66.43°. The right shift of the peaks means that the addition of fluorine reduces the lattice parameters of the matrix compared with that of the pure ZnO nanocomposites with the same amount of nanofiller. Only one ZnO main peak shifts with the addition of fluorine, indicating that fluorine can be incorporated into the ZnO lattice without affecting the lattice parameter of ZnO significantly. Formation of ZnF_2 may lead to a reduce of crystal size resulting in the ZnO appearing under compression [62]. In the case of nitrogen doping, both PVDF and ZnO peaks present an overall left shift. The PVDF peaks shift to 20.20°, 18.45° and 39.24° and the ZnO peaks to 31.67°, 34.44° and 36.36°. The peaks corresponding to planes (−2 2 1) and (1 1 1) shift to 41.26° and 22.63°. Only two peaks show a 0.03–0.04° right shift. Overall, these results indicate that the addition of nitrogen causes expansion of the crystal structure of the ZnO. This might be explained by the mainly interstitial incorporation of N since it has greater ionic radii compare with Zn and O.

Fig. 4 presents the element spectrum of pure and doped nanoparticles. According to Fig. 4 (a), the pure ZnO nanoparticles were successfully synthesized without any impurities. The small amounts of carbon and gold originate from the carbon adherent and surface coating used to fix the powder onto the substrate and make the surface conductive. The fluorine and nitrogen peaks in Fig. 4 (b) and (c) indicate the successful doping of the nanoparticles. The element spectra show that doped nanoparticles present some impurities. Sodium, sulphur and phosphorus are present in the F and N doped nanoparticles. The

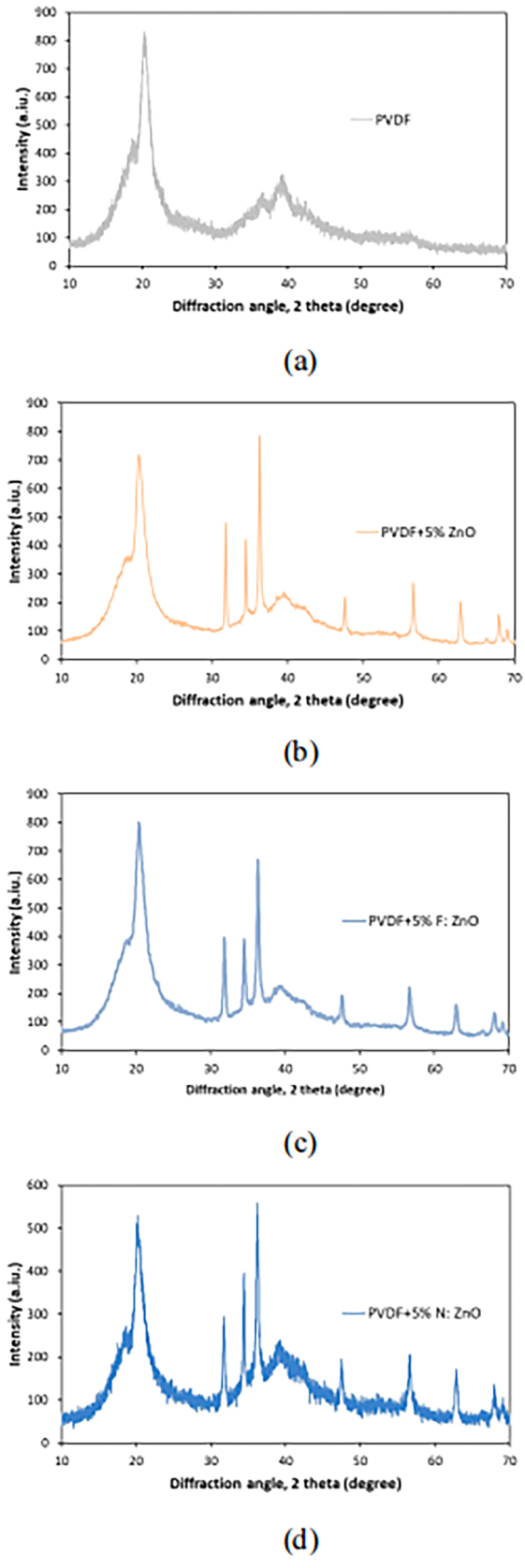

Fig. 3. XRD spectra of PVDF and nanocomposites with and without dopants: (a) PVDF; (b) PVDF + 5 wt% ZnO; (c) PVDF + 5 wt% F:ZnO; (d) PVDF + 5 wt% N: ZnO.

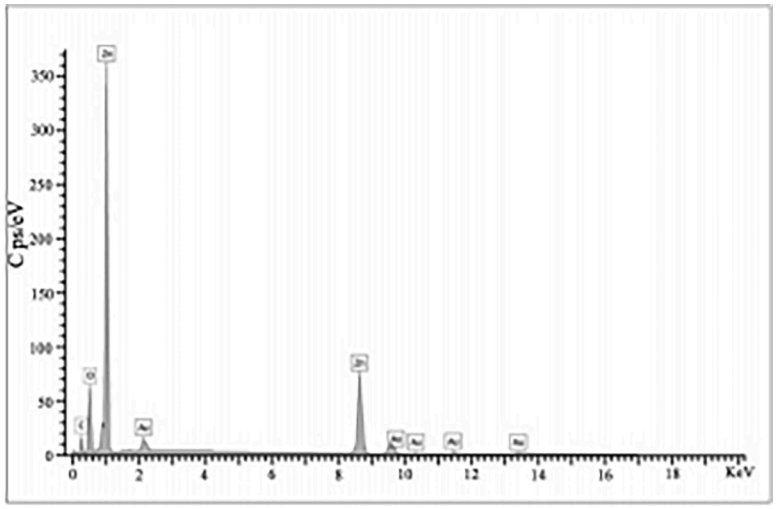

(a)

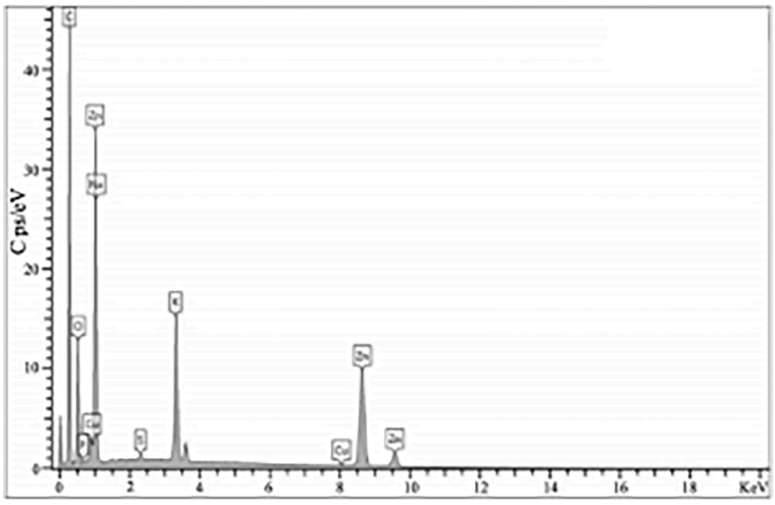

(b)

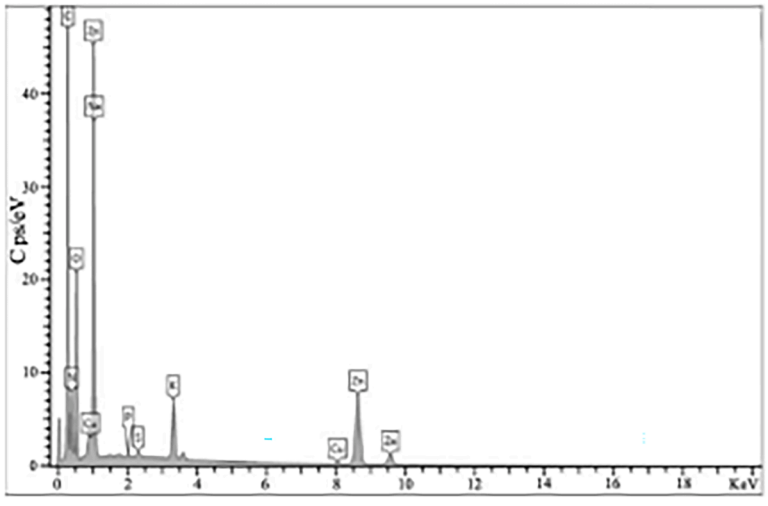

(c)

Fig. 4. Element spectra of (a) pure ZnO nanoparticles; (b) F-doped ZnO nanoparticles; and (c) N-doped nanoparticles.

potassium originates from the agent used to prepare the nanoparticles; the K is extracted from the KOH.

Fig. 5 presents SEM images of pure ZnO and doped nanoparticles; the images also indicate the nanoparticles size. The nanoparticles change from spherulite like to rod like with the addition of dopant. The pure ZnO nanoparticles are around 100–150 nm in diameter, while the length of particles increases to 300–600 nm and the width decreases to 60–70 nm with the addition of fluorine and nitrogen. The variation of the morphology could be due to the presence ammonium fluoride which generates more hydroxide ions that can increase the aspect ratio of nanofillers with zinc ion [63].

Fig. 6 shows SEM images of the pure PVDF and nanocomposites with and without doping. The PVDF shows a porous and spherulitic microstructure in both pure PVDF and nanocomposites indicating that the α phase is dominant [50]. The addition of nanofiller does not change the morphology of the matrix as the PVDF in the nanocomposites is still dominated by the α phase. The spherulite size increases significantly from about 12 μm to nearly 16 μm after adding 5 wt% of ZnO; the growth of spherulites represents the reduction of non-crystalline regions. In the nanocomposites, the spherulite size increase is attributed to the ZnO promoting the crystallisation of PVDF by acting as a nucleating agent and triggering crystal growth, which is consistent with the observation that pure ZnO nanocomposites present higher melting temperature and greater crystallinity with the addition of ZnO. A change of spherulite size can be observed in nanocomposites with dopants. The doped nanocomposites present smaller spherulite size than undoped materials. For the nanocomposite with 5 wt% F-doped ZnO, the spherulite size decreases to about 11 μm, whilst the N-doped nanocomposite with the same loading amount has a spherulite size of around 9 μm. The reduction in the spherulites size with doping can be attributed to a limited crystal growth space.

Fig. 7 illustrates the element distribution of nanocomposites with 15 wt% nanofiller. Small areas of aggregation can be observed after addition of 15 wt% of ZnO in PVDF. The aggregation of the nanocomposites is reduced with the addition of fluorine; the nanocomposites with 15 wt % F-doped ZnO still present some aggregation, but with smaller size and density. In the nitrogen case, the nanocomposites present more aggregation areas than in pure ZnO nanocomposites. Also, the nitrogen doped materials present a lower Zn distribution density than pure ZnO nanocomposite, indicating that there is aggregation areas at other places of the nanofilm.

3.4. Dielectric response

The dielectric constant and loss spectra of pristine PVDF and nanocomposites with and without dopants are illustrated in Figs. 8 and 9. Both dielectric constant and loss decrease with increasing frequency. The dielectric spectra of nanocomposites with dopants present a greater slope than pure ZnO nanocomposites especially for the material with 15 wt% F-doped ZnO. At room temperature, the dielectric loss decreases

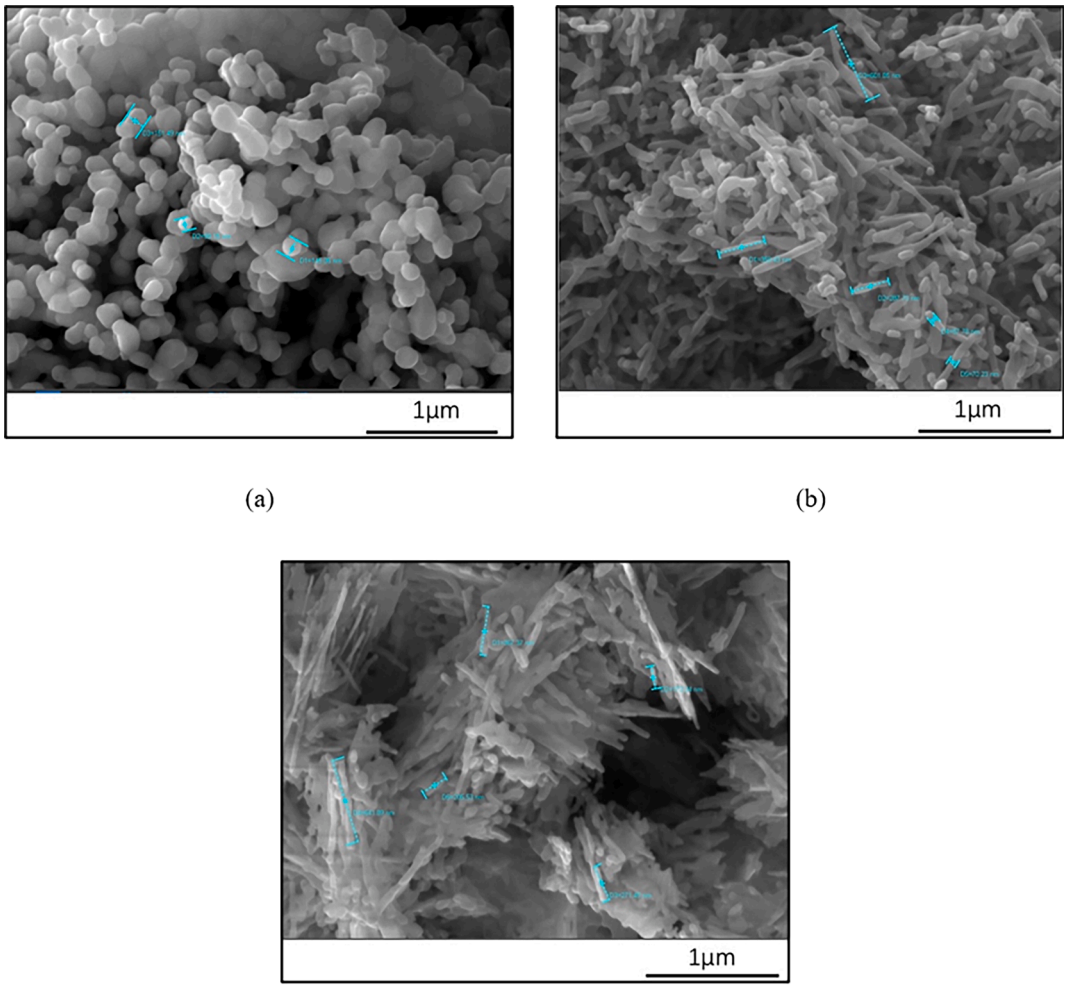

Fig. 5. SEM images of (a) pure ZnO nanoparticles (b) F-doped nanoparticles and (c) N-doped nanoparticles.

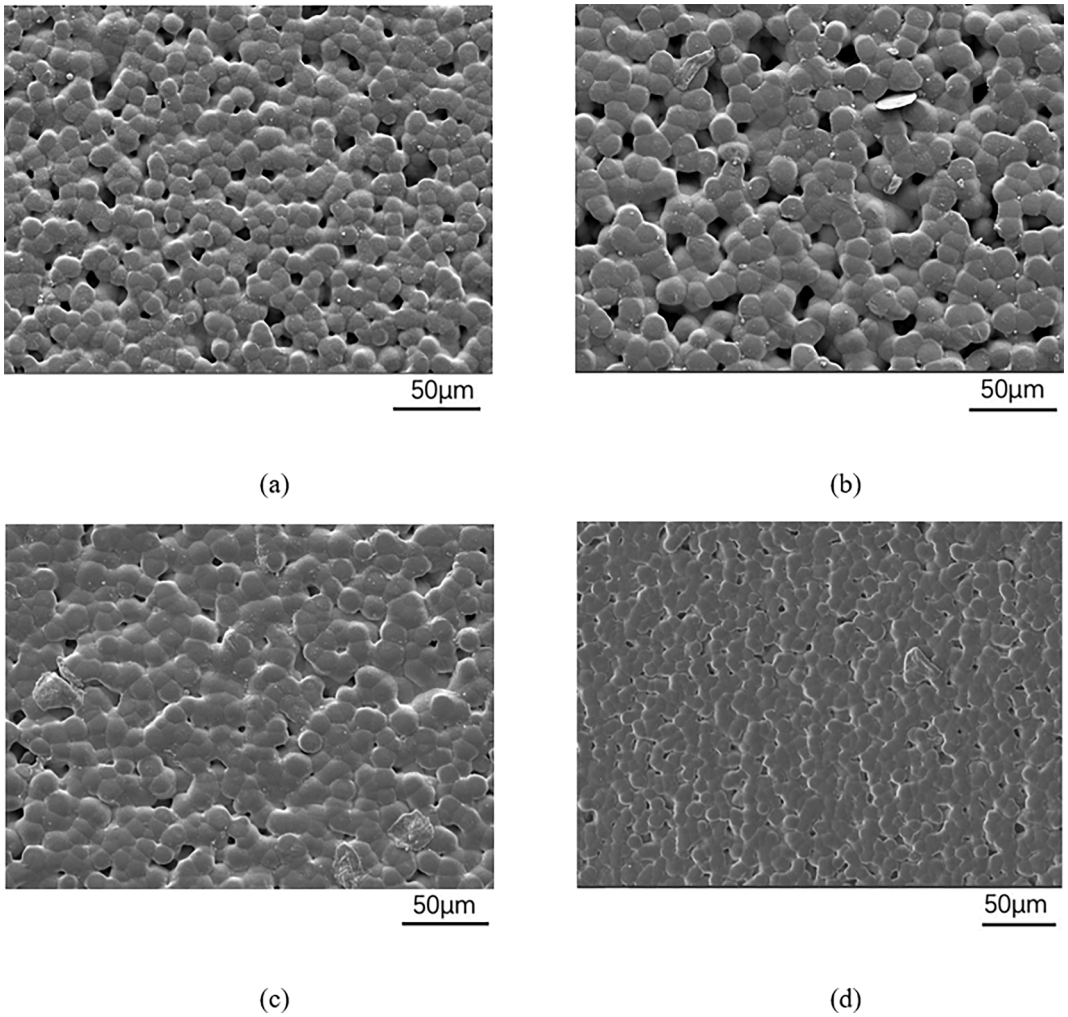

Fig. 6. SEM images of (a) PVDF (b) PVDF + 5 % wt ZnO (c) PVDF + 5 wt% F: ZnO and (d) PVDF + 5 wt% N: ZnO.

with frequency and increases again. With the increase of temperature, the spectra of dielectric constant and loss become steeper. The variation of dielectric constant and loss with frequency is due to the different relaxation mechanisms present in the materials. These include the α relaxation in the crystalline region which mainly occurs at about 1 Hz [64], and explains the high dielectric constant and loss at low frequency. The dielectric loss increase in the high frequency range indicates a second relaxation peak corresponding to the α relaxation in the amorphous region located in the 1–10 MHz range [64]. The interfacial Maxwell-Wagner-Sillars polarisation expected for the systems with ceramic nanoparticles is not detected in Fig. 7 or 8, as it occurs at frequencies below the lower limit of the spectra shown here at about 1 MHz [64]. However, the greater slope of dielectric spectra of nanocomposites with dopant is indicative of a shift of the MWS mechanism towards higher frequencies. The addition of dopants decreases the relaxation time leading to greater relaxation frequency, thus shifting the dielectric spectra to the right.

Fig. 8 shows that the introduction of ZnO enhances the dielectric constant of the nanocomposites significantly. The dielectric constant at room temperature at 10 Hz increases from about 12 for the pristine PVDF to 15 when 5 wt% ZnO is added, and further increases to 17 when 15 wt% of nanoparticles is added; this trend follows previous results for PVDF/ZnO nanocomposites [31]. Pure ZnO nanocomposites present lower dielectric loss than pristine PVDF at room temperature. The dielectric loss of nanocomposite with 5 wt% ZnO is about 2.6 at room temperature and 10 Hz, whilst for the PVDF it is about 3.8 at the same frequency and temperature. The dielectric loss of the material with 15 wt% ZnO is about 2.2 at the same conditions, which show that the loss decreases with increasing nanofiller content. The increase of permittivity with the addition of ZnO nanoparticles is mainly due to an increase in migrating charges [65] and interfacial polarisation. Also, the decrease of inter-dipolar distance at the interface area could be affecting the dielectric response [66]. The orientation of the polymer and nanofiller interfacial charges contributes to polarisation increasing the dielectric constant with the increase of nanofiller amount. The lower dielectric loss of pure ZnO nanocomposites than that of pristine PVDF is due to mobility limitations; the nanoparticles restrict the motion of polymer chains, which increases the relaxation time, and shifts the relaxation to lower frequencies. Consequently, nanocomposites with higher ZnO content show lower dielectric loss.

The addition of dopants further enhances the dielectric constant of nanocomposites as it can be observed in Fig. 8. At room temperature with 15 wt% nanoparticles, the dielectric constant at 10 Hz increases from about 15 for the nanocomposite without fluorine doping to 70 for the material with fluorine. For the N-doped nanocomposites, the dielectric constant of the nanocomposite with 15 wt% nanofiller increases to 35 for the material. Unlike the pure ZnO nanocomposites, F-doped nanofilms present a dielectric loss significantly higher than that of the pure polymer and of ZnO containing films which increases with the nanofiller amount at all frequencies and temperatures. Nanocomposites with 15 wt% N-doped ZnO show greater dielectric loss at room temperature than that of the corresponding undoped material, while the

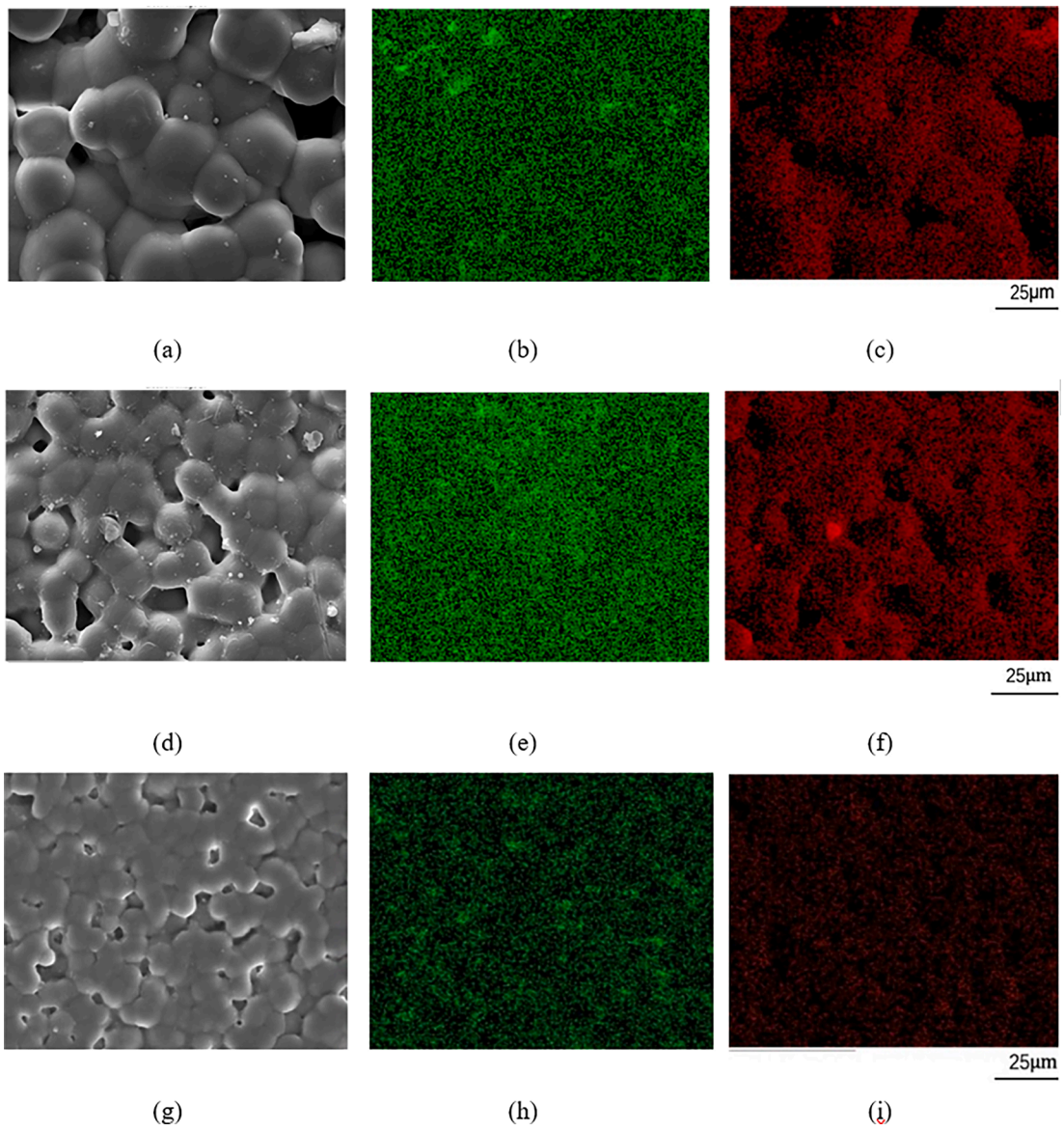

Fig. 7. (a) SEM image of PVDF + 15 wt% ZnO; (b) Zn distribution of PVDF + 15 wt% ZnO; (c) O distribution of PVDF + 15 wt%; (d) SEM image of PVDF + 15 wt% F: ZnO; (e) Zn distribution of PVDF + 15 wt% F: ZnO; (f) O distribution of PVDF + 15 wt% F:ZnO; (g) SEM image of PVDF + 15 wt% N:ZnO; (h) Zn distribution of PVDF + 15 wt% N:ZnO; and (i) O distribution of PVDF + 15 wt% N:ZnO.

other N-doped nanocomposites present similar dielectric loss with that of the pure ZnO material. For example, the loss of the material with 10 wt% nanofiller is about 0.13 at room temperature and 10 Hz both with and without nitrogen doping.

The increase of temperature greatly enhances the dielectric constant and loss of pristine PVDF and nanocomposites. By comparing Fig. 8 (a) and (d), it can be observed that the dielectric constant of nanocomposite with 15 wt% ZnO nanofiller at 10 Hz increases from about 15 at room temperature to about 100 at 100 °C, while the constant of pure PVDF also increases from 12 to 70 in the same conditions. The dielectric constant of the material with 5 wt% of ZnO increases to around 200 when the temperature reaches 100 °C. Nanocomposites with lower pure ZnO content present greater constant at low frequencies with the increase of temperature, especially at 100 °C. This is attributed to the effects of restriction nanoparticles impose to the polymer chain. This leads to an increase of relaxation time and a lower relaxation frequency. Therefore, the dielectric constant spectra of nanocomposites shift to the left with the increase of ZnO. The nanocomposite with 15 wt% F-doped ZnO presents the highest dielectric constant amongst all materials at 100 °C and 10 Hz, which is around 500. The nanocomposite with the same amount of N-doped ZnO has a constant of around 180, which is lower than the nanocomposite with 5 wt% of pure ZnO at the same temperature and frequency. This could be attributed to the weaker temperature dependence of the dielectric properties of N-doped materials. The highest dielectric loss is observed for the nanocomposite with 15 wt% F-doped ZnO and is around 2000 at 100 °C and 10 Hz. This is about 6 times greater than that of the pure ZnO nanocomposites with the same nanofiller amount under the same conditions. When the temperature increases, especially at 75 °C, the dielectric loss values of nanocomposites with 15 wt% N-doped ZnO and 5 wt% pure ZnO are similar at 10 Hz at around 125 and 85 respectively, and nearly overlap at a value of 430 when the temperature increases to 100 °C.

Fig. 10 illustrates the imaginary modulus spectra of pristine PVDF and nanocomposites which can facilitate the identification of relaxation peak shifts. At room temperature, only the relaxation peak of the F-doped nanocomposites with 10 wt% and 15 wt% of nanofiller can be observed which evidences the right shift with fluorine doping. At 50 °C, the relaxation peak of pure PVDF and N-doped nanocomposite with 15

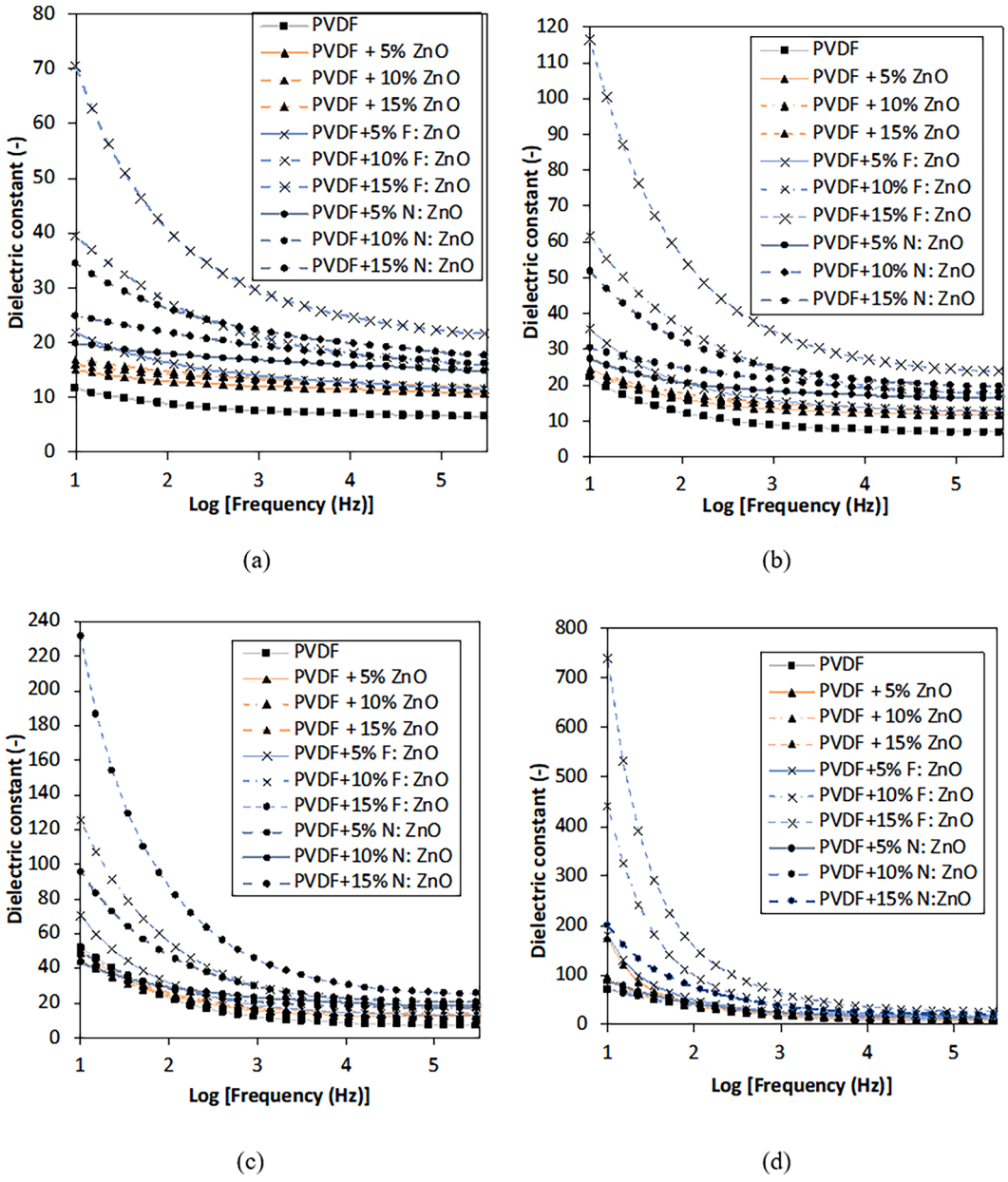

Fig. 8. Dielectric constant spectra of nanocomposites at (a)25 °C (b)50 °C (c)75 °C and (d)100 °C.

wt% of nanofiller can also be observed, while the complete relaxation peak cannot be observed for pure ZnO nanocomposites. This supports the conclusion that the addition of ZnO results in a left shift of the spectrum, which is enhanced with increasing nanofiller amount. The manifestation of the relaxation peak of N-doped nanocomposites evidences the right shift of the spectrum with the application of nitrogen. However, with the increase of temperature, the pure ZnO nanocomposites present greater relaxation frequency than N-doped materials. This indicates that the pure ZnO nanocomposites have a stronger temperature dependence than the N-doped nanocomposites.

Fig. 11 summarizes the dielectric constant of polymer-based nanocomposites at 1 kHz and compares with the state of the art in the literature [67–71]. The nanocomposites with 7 % $NaNbO_3$@Al_2O_3, 9 % BTO@TiO2@SiO2 and 15 % ZnO present similar dielectric constant with the nanocomposite containing 10 wt% F-doped ZnO from this work. Compared to the nanocomposite from the literature that also uses ZnO as nanofiller but co-polymer as matrix [70], the F-doped nanocomposite requires a lower amount of nanofiller to achieve the same level of dielectric constant enhancement. The other two nanocomposites from the literature which use a core–shell structured nanofiller [67,69] that requires a comparatively complex synthesis procedure do not show a significant advantage over the F-doped material from this work. The nanocomposite with 15 wt% F-doped ZnO shows similar dielectric constant to the materials that contains Ag nanoparticles and surface modified $BaTiO_3$ from the literature [68,71]. The F-doped nanocomposite from this work requires a significantly lower amount of nanofiller to achieve the same dielectric constant. The N-doped nanocomposite with 15 wt% nanofiller shows lower dielectric constant than the F-doped nanocomposite and the state of the art materials. However, due to the difference in the nanofiller amount, it is still possible that the N-doped nanocomposite can achieve greater dielectric constant than the state of the art materials in the literature if the same amount of nanofiller is used.

Fig. 12 summarizes the tanδ values of the nanocomposites at 1 kHz and compares them with the state of the art materials from the literature. Both F-doped and N-doped nanocomposites present a much higher tanδ

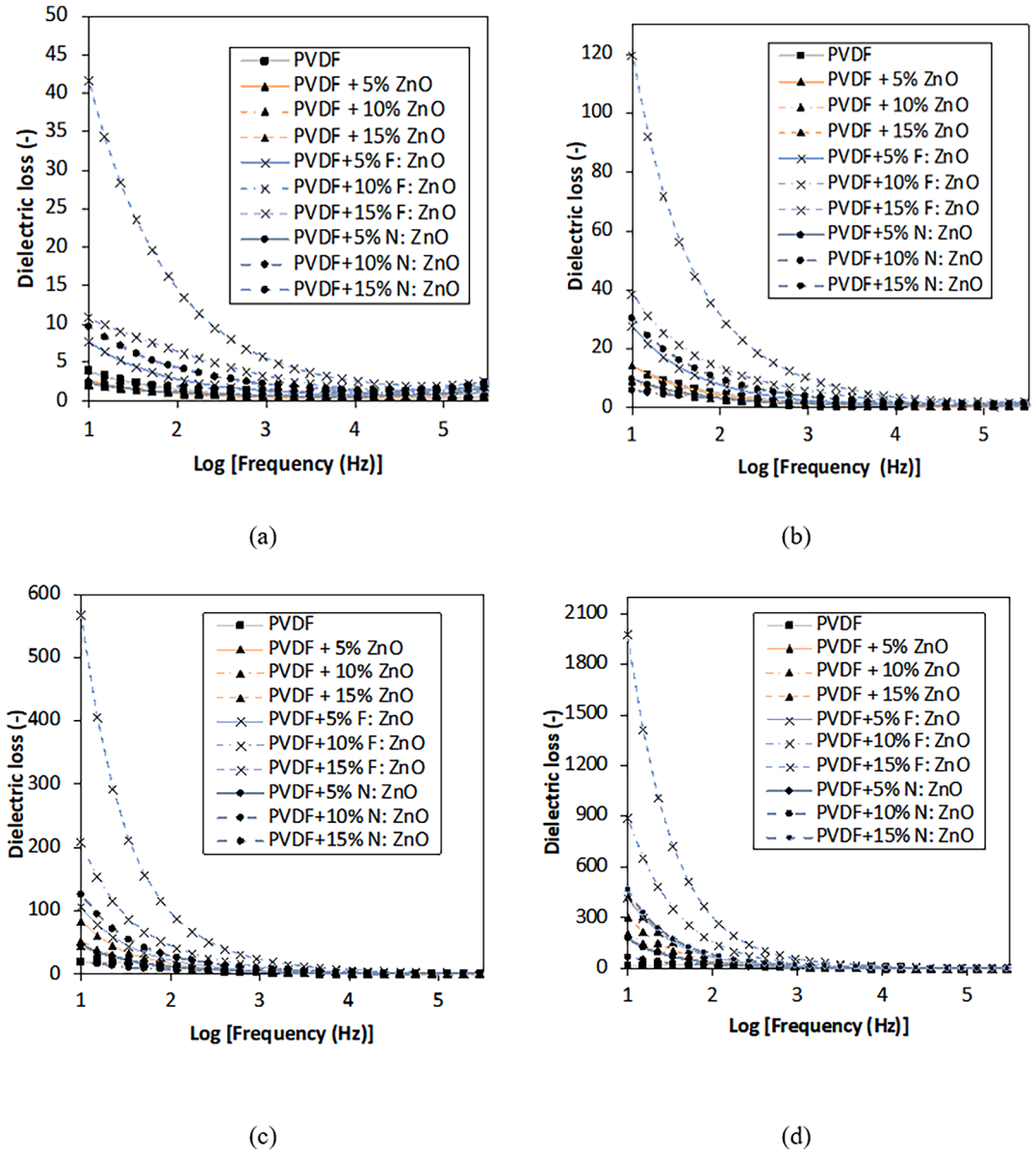

Fig. 9. Dielectric loss spectra of nanocomposites at (a) 25 °C (b) 50 °C (c) 75 °C and (d) 100 °C.

than the materials in the literature. The tanδ of the materials in the literature is around 0.05 while the F-doped nanocomposite shows tanδ nearly 6 times higher. The tanδ of the nanocomposite with 15 % F-doped ZnO is nearly 10 times higher than the materials in previous studies, although 60 % of nanofiller is used in this case. The nanocomposite with 25 % AgNP@DPA shows a tanδ close to the nanocomposite with 10 % F-doped ZnO which is around 0.3 and about half of that of the material with 15 % F-doped ZnO. N-doped nanocomposites present a lower tanδ than F-doped materials.

Materials used for dielectric energy storage devices require a high energy density which can be achieved by either enhanced dielectric constant or breakdown strength. Also, a low dielectric loss is necessary as it represents greater efficiency and longer life. The nanocomposites reported here can achieve higher than or similar level of dielectric constant as the current state of the art by much easier preparation procedures and/or lower nanofiller amount. The enhancement using fluorine and nitrogen is due to the increase in the charge carriers concentration. More charges can be transferred into the nanostructure when the electric field is applied; these charges are than blocked by the insulator polymer at the interface region, which enhances the polarisation and thus increases the dielectric constant. However, the charge mobility can also be enhanced and can cause greater energy dissipation resulting in increased dielectric loss. The nitrogen doped nanocomposites show a controlled increase of dielectric loss due to the decline of migrating charges mobility when the nitrogen is added [72].

Fig. 13 compares Arrhenius plots of relaxation time of pure PVDF and nanocomposites with and without dopant. The relaxation time as a function of temperature follows Arrhenius behavior. The crystalline relaxation process follows a straight line in log scale indicating that both the PVDF and nanocomposite undergo a single rate activation process. Therefore, the activation energy can be determined by the slope of the line and the Arrhenius relation:

$$f = f_o \exp\left(-\frac{E_a}{kT}\right) \tag{4}$$

where f is the relaxation freuqnecy, E_a is the activation energy and k is the Boltzmann constant which is equal to 1.38×10^{-23} $m^2kgs^{-2}K^{-1}$ and T the temperature in K. The activation energy is 0.41 eV for pure PVDF and 0.37 eV for the nanocomposite with 5 wt% ZnO. The lower activation energy for the nanocomposite means that the relaxation is more

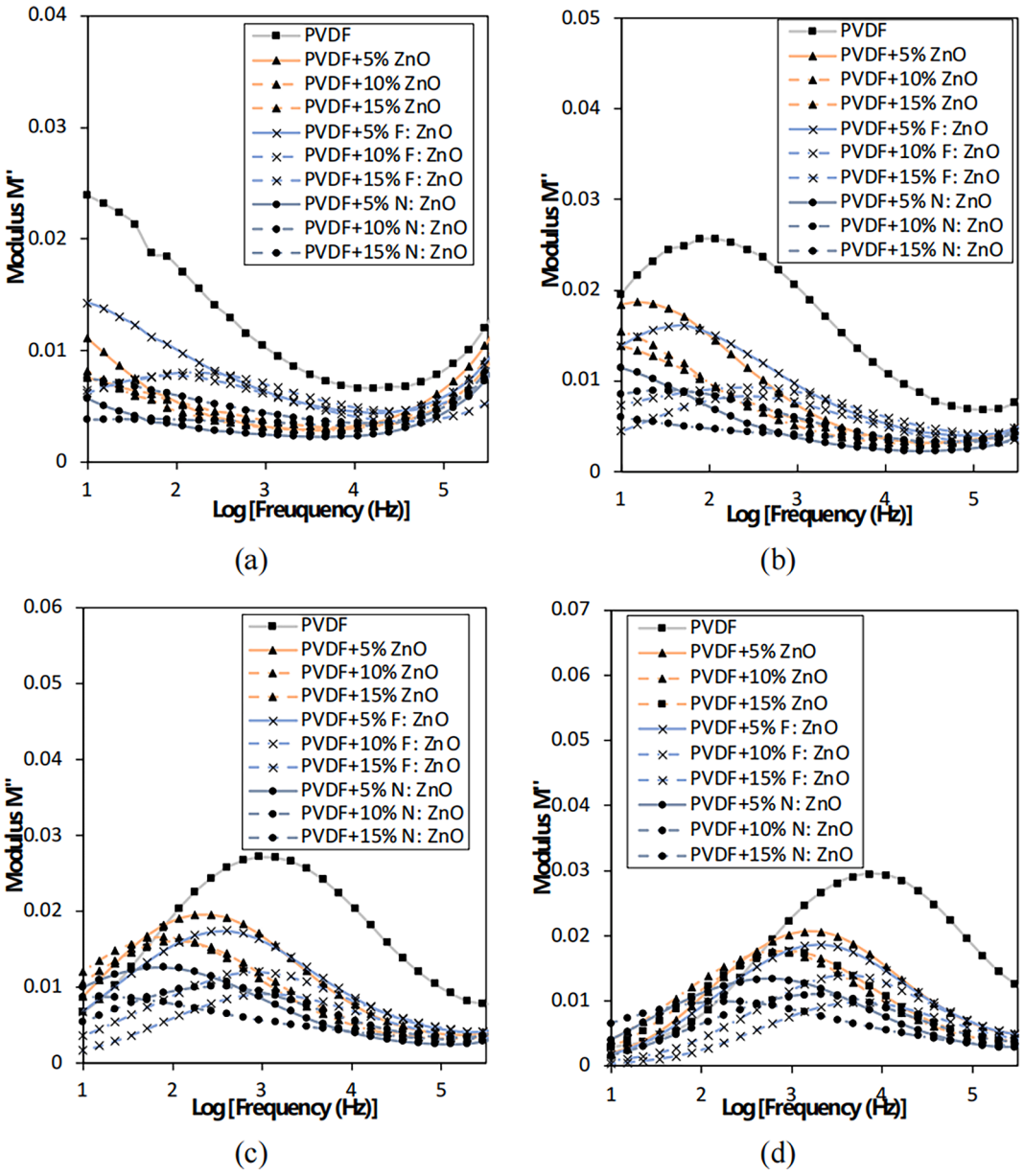

Fig. 10. Imaginary modulus spectra of nanocomposites at (a) 25 °C (b) 50 °C (c) 75 °C and (d) 100 °C.

sensitive to temperature and the process requires lower energy to overcome the energy barrier. Thus, the nanocomposites present a greater dielectric loss at high temperature. The activation energy of F-doped nanocomposites is 0.34 eV which is significantly lower than the value observed for the neat PVDF and ZnO nanocomposite respectively, whilst the activation energy of N-doped nanocomposite with 5 wt% nanofiller is 0.40 eV, which is higher than the value for the pure ZnO nanocomposite. The low activation energy of F-doped nanocomposite is consistent with the result that the F-doped nanocomposite exhibit the highest dielectric constant and loss among all the nanocomposites with the same loading amount, while the activation energy of N-doped nanocomposite explains the result that its dielectric constant is close to that of pure ZnO nanocomposites at high temperature.

4. Conclusion

Addition of ZnO enhances the thermal stability of PVDF and addition of dopants improves further the thermal characteristics of the nanocomposites. Nitrogen doping increases the decomposition temperature to 465 °C which is the highest value among all the nanocomposites studied whilst fluorine improves both the decomposition temperature and weight loss. ZnO also promotes the crystallisation of the PVDF; the increase of ZnO content results in increased numbers of crystallites with smaller size. Fluorine doping of ZnO further promotes the crystallisation of nanocomposites and the crystallinity increases with the increase of F-doped ZnO to 65 %, whilst nitrogen doping influences the crystallisation negatively with a reduction of crystallinity to 48 % with 15 wt% of N-doped ZnO. The addition of ZnO results in higher dielectric constant and lower dielectric loss than pure PVDF. Both fluorine and nitrogen increase the dielectric constant and dielectric loss. Pure PVDF presents the highest activation energy of 0.41 eV and thus has the lowest dielectric constant and loss at high temperature. The activation energy of the F-doped nanocomposite with 5 wt% nanofiller is only 0.34 eV, and therefore this material has the greatest temperature dependence of dielectric properties.

The results reported here indicate the potential of using doping to tailor and optimise the properties nanocomposites for dielectric storage applications. Overall, PVDF-ZnO nanocomposites have to potential of

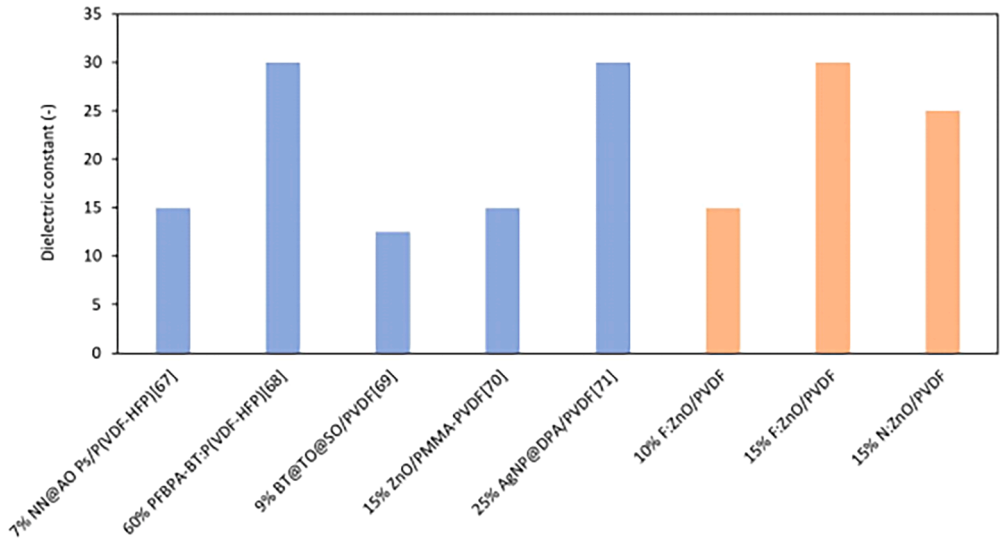

Fig. 11. Summary of dielectric constant of polymer-based nanocomposites at 1 kHz and comparison with literature data.

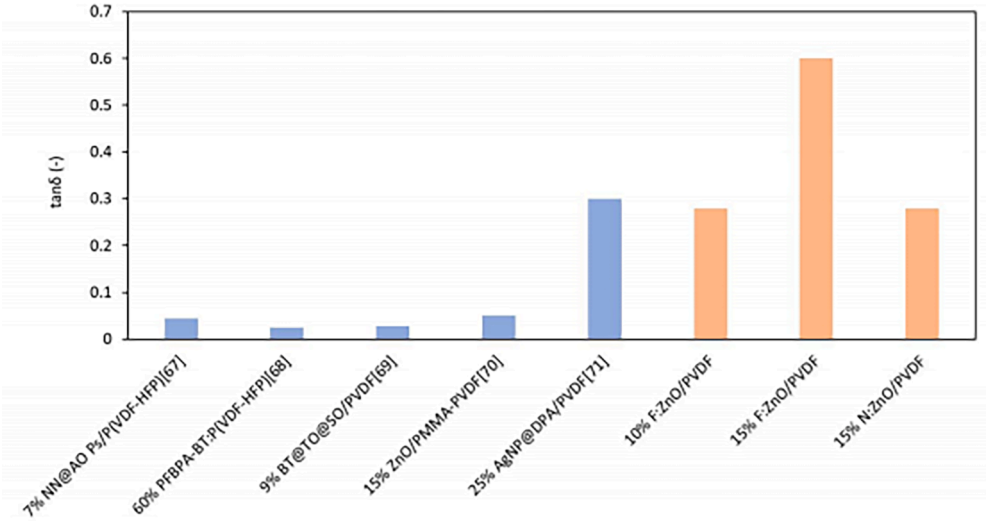

Fig. 12. Summary of tan δ of polymer-based nanocomposites at 1 kHz and comparison with literature data.

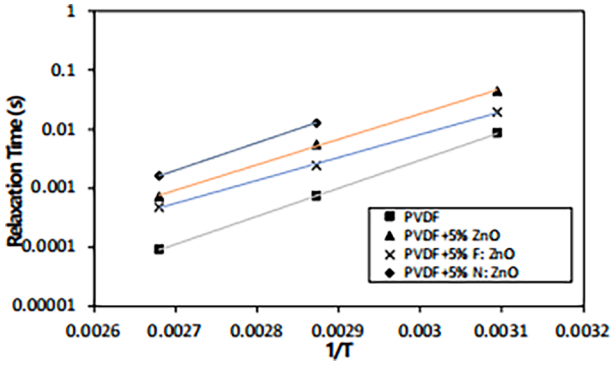

Fig. 13. Arrhenius plot for crystalline relaxation of neat PVDF and nanocomposite with and without adding dopants.

providing an efficient solution in dielectric capacitors as energy storage devices. They show enhanced dielectric constant and reduced dielectric loss due to the restriction ZnO imposes on the polymer chain of PVDF. The addition of fluorine and nitrogen further enhances the dielectric constant of the nanocomposites. However, the addition of fluorine also increases the dielectric loss especially at high temperature. Nitrogen doping does not increase the dielectric constant to the same level as fluorine; however, nitrogen doped nanocomposites present a controlled increase of dielectric loss even at high temperature. The dielectric loss of nanocomposites with nitrogen doping is close or even lower than that of pure ZnO nanocomposites due to the reduction of charge mobility. Apart from dielectric properties, the thermal stability is enhanced with the addition of fluorine and nitrogen. Fluorine doped nanocomposites present increased thermal decomposition temperature and reduced polymer weight loss. Nitrogen doped nanocomposites present the highest decomposition and inflection temperature among all materials. Fluorine improves the interface between the nanofiller and matrix, resulting in increased crystallinity, whilst nitrogen does not influence the interface positively but increases the melting temperature.

To further enhance the overall performance of the nanocomposites, the two dopants can be combined in co-doped formulations and to utilize the advantages of fluorine and nitrogen in a synergistic manner. The opportunity offered by the differing influence of dopants of different electronegativity and size can be used to address the trade-off governing material development and selection for dielectric storage. A broader

investigation including the influence of doping of nanoparticles on dielectric breakdown will establish the full potential of this material solution.

CRediT authorship contribution statement

Shuyang Chen: Formal analysis, Investigation, Methodology, Writing – original draft. **Vijay Kumar Thakur:** Conceptualization. **Alexandros A. Skordos:** Supervision, Writing – review & editing.

Declaration of competing interest

The authors declare that they have no known competing financial interests or personal relationships that could have appeared to influence the work reported in this paper.

Data availability

The link to access the data is inlcuded at the end of the paper

Acknowledgement

The help of Christine Kimpton on SEM, Jim Hurley on the dielectric setup and processing and of Dr David Ayre on TGA and DSC training are gratefully acknowledged. The work was not funded by any organization.

Ethical approval

There is no conflict of interest of all the co-authors and no human/animal tissues has been applied in this work.

Data availability statement

The raw data required to reproduce these findings are available to download from the link attached [http://doi.org/10.17862/cranfield.rd.22786217] [49]. The link contains the original data of TGA, DSC, XRD and dielectric measurements.

References

[1] M. Ji, D.Y. Min, L. Li, Q. Yang, W Liu Wu, S. Li, Improved energy storage performance of polyimide nanocomposites by constructing the meso- and macroscopic interfaces, Mater. TodayEnergy 31 (2023), https://doi.org/10.1016/j.mtener.2022.101200.

[2] Y. Arfat, S.P. Singh, S. Arya, S. Khan, Modelling, design and parametric considerations for different dielectric materials on substrate integrated waveguide, Wseas Trans. Commun. 13 (2014) 94–98.

[3] G. Liu, H. Fan, J. Xu, Z. Liu, Y. Zhao, Colossal permittivity and impedance analysis of niobium and aluminum co-doped TiO2 ceramics, RSC Adv. 6 (54) (2016) 48708–48714, https://doi.org/10.1039/c6ra07746c.

[4] J. Shi, H. Fan, X. Liu, Y. Ma, and Q. Li, "Bi deficiencies induced high permittivity in lead-free BNBT-BST high-temperature dielectrics," *Journal of Alloys and Compounds*, vol. 627. Elsevier Ltd, pp. 463–467, Apr. 05, 2015. doi: 10.1016/j.jallcom.2014.12.022.

[5] V.K. Thakur, E.J. Tan, M.F. Lin, P.S. Lee, Polystyrene grafted polyvinylidenefluoride copolymers with high capacitive performance, Polym. Chem. 2 (9) (2011) 2000–2009, https://doi.org/10.1039/c1py00225b.

[6] S. Verma, B. Padha, S. Young, Y. Chu, R. Bhardwaj, R. Mishra, S. Arya, "3D MXenes for supercapacitors: Current status, opportunities and challenges", Progress in Solid State Chemistry, Elsevier Ltd (2023), https://doi.org/10.1016/j.progsolidstchem.2023.100425.

[7] Y. Bai, V. Bharti, H.S. Xu, Q.M. Zhang, V. Affiliations, High dielectric constant ceramic powder polymers, Appl. Phys. Lett. 76 (25) (2000) 3804–3806, https://doi.org/10.1063/1.126787.

[8] D.H. Kuo, C.C. Chang, T.Y. Su, W.K. Wang, B.Y. Lin, Dielectric behaviours of multi-doped BaTiO3/epoxy composites, J. Eur. Ceram. Soc. 21 (9) (2001) 1171–1177, https://doi.org/10.1016/S0955-2219(00)00327-7.

[9] Z.M. Dang, H.Y. Wang, H.P. Xu, Influence of silane coupling agent on morphology and dielectric property in BaTiO3/polyvinylidene fluoride composites, Appl. Phys. Lett. 89 (11) (2006) 87–90, https://doi.org/10.1063/1.2338529.

[10] Z.M. Dang, H.Y. Wang, B. Peng, C.W. Nan, Effect of BaTiO3 size on dielectric property of BaTiO 3/PVDF composites, J. Electroceram. vol. 21, no. 1–4 SPEC. ISS (2008) 381–384, https://doi.org/10.1007/s10832-007-9201-8.

[11] P. Mahajan, S. Verma, B. Padha, A. Ahmed, S. Arya, Manganese oxide and nickel oxide thin films on polyester to enable self-charging wearable supercapacitor, J. Alloy. Compd. 968 (Dec. 2023), https://doi.org/10.1016/j.jallcom.2023.171904.

[12] J. Wang, J. Hu, L. Yang, K. Zhu, B. Li, Q. Sun, Y. Li, J. Qiu, High discharged energy density of polymer nanocomposites induced by Nd-doped BaTiO3 nanoparticles, J. Materiomics 4 (1) (2018) 44–50, https://doi.org/10.1016/j.jmat.2018.01.001.

[13] M.F. Lin, V.K. Thakur, E.J. Tan, P.S. Lee, Dopant induced hollow BaTiO3 nanostructures for application in high performance capacitors, J. Mater. Chem. 21 (41) (2011) 16500–16504, https://doi.org/10.1039/c1jm12429c.

[14] P. Kum-onsa, N. Chanlek, J. Manyam, P. Thongbai, V. Harnchana, N. Phromviyo, P. Chindaprasirt, Gold-nanoparticle-deposited TiO2 nanorod/poly(Vinylidene fluoride) composites with enhanced dielectric performance, Polymers (basel) 13 (13) (2021) 1–14, https://doi.org/10.3390/polym13132064.

[15] V.K. Thakur, M.F. Lin, E.J. Tan, P.S. Lee, Green aqueous modification of fluoropolymers for energy storage applications, J. Mater. Chem. 22 (13) (2012) 5951–5959, https://doi.org/10.1039/c2jm15665b.

[16] K. Yang, X. Huang, Y. Huang, L. Xie, P. Jiang, Fluoro-Polymer@BaTiO3 Hybrid Nanoparticles Prepared via RAFT Polymerization: Toward Ferroelectric Polymer Nanocomposites with High Dielectric Constant and Low Dielectric Loss for Energy Storage Application, Chem. Mater. 25 (2013) 2327–2338.

[17] Q. M. Z. Baojin Chu, Xin Zhou, Kailiang Ren, Bret Neese, Minren Lin, F. Bauer, "A Dielectric Polymer with high electric energy density and fast discharge speed," *Science (1979)*, vol. 313, no. July, pp. 334–336, 2006, doi: 10.1126/science.1128383.

[18] Y. Liu, H. Luo, D. Zhai, L. Zeng, Z. Xiao, Z. Hu, X. Wang, D. Zhang, Improved Energy Density and Energy Efficiency of Poly(vinylidene difluoride) Nanocomposite Dielectrics Using 0.93Na0.5Bi0.5TiO3-0.07BaTiO3 Nanofibers, ACS Appl. Mater. Interfaces 14 (2022) 19376–19387, https://doi.org/10.1021/acsami.2c00969.

[19] Y. Song, Y. Shen, H. Liu, Y. Lin, M. Li, C.W. Nan, Enhanced dielectric and ferroelectric properties induced by dopamine-modified BaTiO3 nanofibers in flexible poly(vinylidene fluoride-trifluoroethylene) nanocomposites, J. Mater. Chem. 22 (16) (2012) 8063–8068, https://doi.org/10.1039/c2jm30297g.

[20] J. Chon, S. Ye, K. Cha, S. Lee, Y. Koo, J. Jung, Y. Kwon, High-κ dielectric sol-gel hybrid materials containing barium titanate nanoparticles, Chem. Mater. 22 (19) (2010) 5445–5452, https://doi.org/10.1021/cm100729d.

[21] J. Ru, D. Min, M. Lanagan, S. Li, G. Chen, Energy storage properties of polyimide/BaTiO3 nanocomposite films and their breakdown mechanism in a wide content range, Appl. Phys. Lett. 115 (21) (2019) pp, https://doi.org/10.1063/1.5115766.

[22] J. Li, P. Khanchaitit, K. Han, Q. Wang, New route toward high-energy-density nanocomposites based on chain-end functionalized ferroelectric polymers, Chem. Mater. 22 (18) (2010) 5350–5357, https://doi.org/10.1021/cm101614p.

[23] Z.M. Dang, T. Zhou, S. Yao, J. Yuan, J. Zha, H. Song, J. Li, Q. Chen, W. Yang, J. Bai, Advanced calcium copper titanate/polyimide functional hybrid films with high dielectric permittivity, Adv. Mater. 21 (20) (2009) 2077–2082, https://doi.org/10.1002/adma.200803427.

[24] X.M. Sui, C.L. Shao, Y.C. Liu, White-light emission of polyvinyl alcohol/ZnO hybrid nanofibers prepared by electrospinning, Appl. Phys. Lett. 87 (11) (2005) pp, https://doi.org/10.1063/1.2048808.

[25] M. Xiong, G. Gu, B. You, L. Wu, "Preparation and Characterization of Poly (styrene butylacrylate), Latex / Nano-ZnO Nanocomposites" 90 (7) (2003) 923–1931.

[26] D. Kaur, A. Bharti, T. Sharma, C. Madhu, Dielectric Properties of ZnO-Based Nanocomposites and Their Potential Applications, Int J Opt 2021 (2021), https://doi.org/10.1155/2021/9950202.

[27] S. Khan, S. Arya, S. Kumar, P. Lehana, Fabrication and characterization of highly sensitive ZnO/Si SAW device with Pd selective layer for F2 gas sensing, Microsyste Technologies 21 (9) (Sep. 2015) 2011–2017, https://doi.org/10.1007/s00542-014-2277-6.

[28] H. Tian, H. Fan, M. Li, L. Ma, Zeolitic Imidazolate Framework Coated ZnO Nanorods as Molecular Sieving to Improve Selectivity of Formaldehyde Gas Sensor, ACS Sens 1 (3) (Mar. 2016) 243–250, https://doi.org/10.1021/acssensors.5b00236.

[29] S. Verma, P. Mahajan, B. Padha, A. Ahmed, S. Arya, Nanowires based solid-state asymmetric self-charging supercapacitor driven by PVA–ZnO–KOH flexible piezoelectric matrix, Electrochim. Acta 465 (Oct. 2023), https://doi.org/10.1016/j.electacta.2023.142933.

[30] C. Madhu, I. Kaur, N. Kaur, Synthesis and investigation of photonic properties of surface modified ZnO nanoparticles with imine linked receptor as coupling agent-for application in LEDs, J. Mater. Sci. Mater. Electron. 28 (9) (2017) 6388–6398, https://doi.org/10.1007/s10854-016-6323-2.

[31] P.I. Devi, K. Ramachandran, Dielectric studies on hybridised PVDF-ZNO nanocomposites, J. Exp. Nanosci. 6 (3) (2011) 281–293, https://doi.org/10.1080/17458080.2010.497947.

[32] A. Jana, T.K. Kundu, Microstructure and dielectric characteristics of Ni ion doped BaTiO3 nanoparticles, Mater. Lett. 61 (7) (2007) 1544–1548, https://doi.org/10.1016/j.matlet.2006.07.075.

[33] Y. Sim, S. Surendran, H. Cha, H. Choi, M. Je, S. Yoo, D. Chan, Y. Ho, C. Jeon, D. Jin, M. Han, H. Choi, U. Sim, J. Moon, Fluorine-doped graphene oxide prepared by direct plasma treatment for supercapacitor application, Chem. Eng. J. 428 (April) (2022) 132086, https://doi.org/10.1016/j.cej.2021.132086.

[34] W. Xu, C. Qin, S. Zhang, H. Liang, W. Lei, Z. Luo, A. Lu, Thermal, structural and electrical properties of fluorine-doped Li3.6Al0.8Ti4.0P7.6O30-x/2Fx (x = 0, 0.5, 1, 2) glass-ceramic electrolytes, J. Alloy. Compd. 853 (2021), https://doi.org/10.1016/j.jallcom.2020.157191.

[35] X. Ren, H. Fan, J. Ma, C. Wang, Y. Zhao, S. Lei, Triboelectric nanogenerators based on fluorinated wasted rubber powder for self-powering application, ACS Sustain. Chem. Eng. 5 (2) (Feb. 2017) 1957–1964, https://doi.org/10.1021/acssuschemeng.6b02756.
[36] J. Fang, H. Fan, M. Li, C. Long, Nitrogen self-doped graphitic carbon nitride as efficient visible light photocatalyst for hydrogen evolution, J Mater Chem A Mater 3 (26) (Jul. 2015) 13819–13826, https://doi.org/10.1039/c5ta02257f.
[37] N.A. Bakr, Effect of Fluorine Doping on Structural and Optical Properties of SnO2 Thin Films Prepared by Chemical Spray Pyrolysis Method, Advances in Materials 5 (4) (2016) 23, https://doi.org/10.11648/j.am.20160504.12.
[38] A. C. Güler, B. Dindar, and H. Orücü, "Effect of B or N doping on the dielectric and electrical properties of ZnO at room temperature," Mater Res Express, vol. 6, no. 6, 2019, doi: 10.1088/2053-1591/ab0b83.
[39] S. Pratihar, A. Patra, A. Sasmal, S.K. Medda, S. Sen, Enhanced dielectric, ferroelectric, energy storage and mechanical energy harvesting performance of ZnO-PVDF composites induced by MWCNTs as an additive third phase, Soft Matter 17 (37) (Oct. 2021) 8483–8495, https://doi.org/10.1039/d1sm00854d.
[40] Y. You, S. Chen, S. Yang, L. Li, P. Wang, Enhanced Thermal and Dielectric Properties of Polyarylene Ether Nitrile Nanocomposites Incorporated with BN/TiO2-Based Hybrids for Flexible Dielectrics, Polymers (basel) 15 (21) (2023) Nov, https://doi.org/10.3390/polym15214279.
[41] Zinc Nitrate Hexahydrate 228737 Sigma Aldrich https://www.sigmaaldrich.com/catalog/substance/zincnitratehexahydrate297491019618611?lang=en&region=GB.
[42] Potassium hydroxide 06103 Sigma Aldrich https://www.sigmaaldrich.com/catalog/substance/potassiumhydroxide5611131058311?lang=en&region=GB.
[43] Ammonium fluoride 1011641000 Sigma Aldrich https://www.sigmaaldrich.com/catalog/substance/ammoniumfluoride370412125018l1?lang=en&region=GB.
[44] Urea 8187101000 Sigma Aldrich https://www.sigmaaldrich.com/catalog/product/mm/818710?lang=en&region=GB.
[45] Polyvinylidene fluoride 182702 Sigma Aldrich https://www.sigmaaldrich.com/catalog/substance/polyvinylidenefluoride123452493779911?lang=en&region=GB.
[46] Dimethyl sulfoxide D8418 Sigma Aldrich https://www.sigmaaldrich.com/catalog/substance/dimethylsulfoxide78136768511?lang=en&region=GB.
[47] RS Pro Conductive Paint RS186-3600 RS https://uk.rs-online.com/web/p/electronics-varnishes/1863600.
[48] H. Ghorbani, F. Mehr, H. Pazoki, B. Rahmani, Synthesis of ZnO nanoparticles by precipitation method, Oril Jour of Chem 31 (2) (2015) 1219–1221, https://doi.org/10.13005/ojc/310281.
[49] Shuyang Chen, Vijay Kumar Thakur, Alexandros A. Skordos, Fluorine and Nitrogen doping of Zinc Oxide to enhance dielectric storage of PVDF based particulate composites, Dataset, Cranfield Online Research Data Repository. (2023), https://doi.org/10.17862/cranfield.rd.22786217.
[50] B. Jaleh, A. Jabbari, Evaluation of reduced graphene oxide/ZnO effect on properties of PVDF nanocomposite films, Appl. Surf. Sci. 320 (November) (2014) 339–347, https://doi.org/10.1016/j.apsusc.2014.09.030.
[51] M. Chipara, K. Lozano, A. Hernandez, M. Chipara, TGA analysis of polypropylene-carbon nanofibers composites, Polym. Degrad. Stab. 93 (4) (2008) 871–876, https://doi.org/10.1016/j.polymdegradstab.2008.01.001.
[52] P. Martins, C.M. Costa, M. Benelmekki, G. Botelho, S. Lanceros-Méndez, Interface characterization and thermal degradation of ferrite/ poly(vinylidene fluoride) multiferroic nanocomposites, J. Mater. Sci. 48 (6) (2013) 2681–2689, https://doi.org/10.1007/s10853-012-7063-1.
[53] B. Pedroso Silva Santos, J. Rubio Arias, F. Elias Jorge, R. Ertola Pereira de Deus Santos, R.B. da Dilva Fernandes, L. da Dilva Candido, A. Cesar de Carvalho Peres, E. Gervasoni Chaves, M. Vieira Marques, Preparation, characterization and permeability evaluation of poly(vinylidene fluoride) composites with ZnO particles for flexible pipelines, Polym. Test. 94 (December) (2021) 2020, https://doi.org/10.1016/j.polymertesting.2021.107064.
[54] A. Issa, M. Al-Maadeed, A. Luyt, D. Ponnamma, M. Hassan, Physico-Mechanical, Dielectric, and Piezoelectric Properties of PVDF Electrospun Mats Containing Silver Nanoparticles, C (basel) 3 (4) (2017) 30, https://doi.org/10.3390/c3040030.
[55] K. Tashiro, Crystal Structure and Phase transition of PVDF and related copolymers, 1st Edition, CRC Press, Boca Raton, 1995.
[56] A.P. Indolia, M.S. Gaur, Investigation of structural and thermal characteristics of PVDF/ZnO nanocomposites, J. Therm. Anal. Calorim. 113 (2) (2013) 821–830, https://doi.org/10.1007/s10973-012-2834-0.
[57] M.M. Chamakh, M. Mrlik, S. Leadenham, P. Bazant, J. Osicka, M. Almaadeed, A. Erture, I. Kurikta, Vibration sensing systems based on poly(Vinylidene fluoride) and microwave-assisted synthesized ZnO star-like particles with controllable structural and physical properties, Nanomaterials 10 (12) (2020) 1–15, https://doi.org/10.3390/nano10122345.
[58] J. Liu, X. Lu, C. Wu, Effect of preparation methods on crystallization behavior and tensile strength of poly(vinylidene fluoride) membranes, Membranes (basel) 3 (4) (2013) 389–405, https://doi.org/10.3390/membranes3040389.
[59] A. Sanchez-Juarez, A. Tiburcio-Silver, A. Ortiz, E.P. Zironi, J. Rickards, Electrical and optical properties of fluorine-doped ZnO thin films prepared by spray pyrolysis, Thin Solid Films 333 (1–2) (1998) 196–202, https://doi.org/10.1016/S0040-6090(98)00851-7.
[60] X. Cai, T. Lei, D. Sun, L. Lin, A critical analysis of the α, β and γ phases in poly (vinylidene fluoride) using FTIR, RSC Adv. 7 (25) (2017) 15382–15389, https://doi.org/10.1039/c7ra01267e.
[61] Y. Ting, Suprapto, N. Bunekar, K. Sivasankar, and Y. R. Aldori, "Using annealing treatment on fabrication ionic liquid-based PVDF films," Coatings, vol. 10, no. 1, 2020, doi: 10.3390/coatings10010044.
[62] S. Gayathrr, O. Sivaraman, N. Ghosh, S. Sathishkumar, P. Sudhakara, J. Jayaramudu, S. Ray and A. Viswanath, "Investigation of physicochemical properties of Ag doped ZnO nanoparticles prepared by chemical route," Appl. Sci. Lett, vol. 1, no. 1, pp. 8–13, 2015, [Online]. Available: https://researchspace.csir.co.za/dspace/handle/10204/8553.
[63] J. Liu, K. Nagashima, H. Yamashita, W. Mizukami, J. Uzuhashi, T. Hosomi, M. Kanai, X. Zhao, Y. Miura, G. Zhang, T. Takahashi, M. Suzuka, D. Sakai, B. Samransuksamer, Y. He, T. Ohkubo, T. Yasui, Y. Aoki, J. Ho, Y. Baba, T. Yanagida, Face-selective tungstate ions drive zinc oxide nanowire growth direction and dopant incorporation, Commun Mater 1 (1) (2020) 1–2, https://doi.org/10.1038/s43246-020-00063-5.
[64] C.V. Chanmal, J.P. Jog, Dielectric relaxations in PVDF/BaTiO3 nanocomposites, Express Polym Lett 2 (4) (2008) 294–301, https://doi.org/10.3144/expresspolymlett.2008.35.
[65] M.S. Gaur, A.P. Indolia, Thermally stimulated dielectric properties of polyvinylidenefluoride-zinc oxide nanocomposites, J. Therm. Anal. Calorim. 103 (3) (2011) 977–985, https://doi.org/10.1007/s10973-010-1190-1.
[66] N. Bouropoulos, G.C. Psarras, N. Moustakas, A. Chrissanthopoulos, S. Baskoutas, "Optical and dielectric properties of ZnO-PVA nanocomposites", Physica Status Solidi (A) Applications and Materials, Science 205 (8) (2008) 2033–2037, https://doi.org/10.1002/pssa.200778863.
[67] Z. Pan, Q. Ding, L. Yao, S. Huang, S. Xing, J. Liu, J. Chen and H. Zhai, "Simultaneously enhanced discharge energy density and efficiency in nanocomposite films capacitors utilizing two-dimensional NaNbO 3 @Al 2 O 3 platelets," 2019.
[68] P. Kim, N. Doss, J. Tillostson, P. Hotchkiss, M. Pan, S. Marder, J. Li, J. Calame, J. Perry, High energy density nanocomposites based on surface-modified BaTiO 3 and a ferroelectric polymer, ACS Nano 3 (9) (2009) 2581–2592, https://doi.org/10.1021/nn9006412.
[69] F. Wang, H. Luo, D. Zhai, Z. Xiao, L. Zeng, X. Wang, Z. Hu, H. Wang, L. Liu, D. Zhang, Dielectric nanocomposites with high energy density by doping core-double shell structured fillers, Compos. A Appl. Sci. Manuf. vol. 159, no. May (2022) 107019, https://doi.org/10.1016/j.compositesa.2022.107019.
[70] M.I. Mohammed, Dielectric dispersion and relaxations in (PMMA/PVDF)/ZnO nanocomposites, Polym. Bull. 79 (4) (2022) 2443–2459, https://doi.org/10.1007/s00289-021-03606-z.
[71] L. Zhang, S. Yuan, S. Chen, D. Wang, B.Z. Han, Z.M. Dang, Preparation and dielectric properties of core-shell structured Ag@polydopamine/poly(vinylidene fluoride) composites, Compos. Sci. Technol. 110 (Apr. 2015) 126–131, https://doi.org/10.1016/j.compscitech.2015.01.011.
[72] K. Mahmood, S. Bin Park, Growth and conductivity enhancement of N-doped ZnO nanorod arrays, J. Cryst. Growth 347 (1) (2012) 104–112, https://doi.org/10.1016/j.jcrysgro.2012.03.033.

2024-02-20

Fluorine and nitrogen doping of zinc oxide to enhance dielectric storage of PVDF based particulate composites

Chen, Shuyang

Elsevier

Chen S, Thakur VK, Skordos AA. (2024) Fluorine and nitrogen doping of zinc oxide to enhance dielectric storage of PVDF based particulate composites. Materials Science & Engineering B, Volume 302, April 2024, Article number 117244

https://doi.org/10.1016/j.mseb.2024.117244